Mediterranean faunal evolution and biochronological events during the last 24 kyr

Sonda Zouari, Soumaya Boussetta, Giuseppe Siani, Nadine Tisnerat-Laborde, François Thil, Abdelaziz Kallel, Elisabeth Michel, Nejib Kallel

Marine Micropaleontology
May 2021, Volume 165, Pages 101997 (16p.)
https://doi.org/10.1016/j.marmicro.2021.101997
https://archimer.ifremer.fr/doc/00691/80342/

Mediterranean faunal evolution and biochronological events during the last 24 kyr

Zouari Sonda [1, 2, *], Boussetta Soumaya [1], Siani Giuseppe [2], Tisnerat-Laborde Nadine [3], Thil François [3], Kallel Abdelaziz [4], Michel Elisabeth [3], Kallel Nejib [1]

[1] Laboratoire Géoressources, Matériaux, Environnement et changements Globaux (GEOGLOB), Faculté des Sciences de Sfax, Université de Sfax, BP802, 3038 Sfax, Tunisia
[2] Laboratoire Géosciences Paris-Sud (GEOPS), Université Paris-Saclay, 91405 ORSAY, France
[3] Laboratoire des Sciences du Climat et de l'Environnement (LSCE), Gif-sur-Yvette, France
[4] Digital Research Centre of Sfax, Technopark of Sfax, Sfax, Tunisia

* Corresponding author : Sonda Zouari, email address : sonda.zouari91@gmail.com

Abstract :

We generated high-resolution biochronological records in the Mediterranean Sea covering the period extending to the Late-glacial. The present study is based on micropaleontological, sea-surface temperature (SST) and oxygen isotopic analyses performed along three well-dated deep-sea cores: REC13–53, KET80–19 and MD84–641 recovered in the Siculo-Tunisian Strait, Tyrrhenian Sea and Levantine Basin, respectively. The quantitative distributional patterns of planktic foraminifera permitted to identify seven biozones based on the apparition and/or disappearance of the main specific taxa or by their noticeable abundance peaks. Abundance records display that major changes in planktic foraminiferal assemblages have a similar pattern mainly in central and western basins. In particular, four recognized bio-events can be used to establish or to improve the chronology of Mediterranean deep-sea cores. The comparison of the SST estimates and foraminiferal records with those of NGRIP ice-core shows a similarity between the Greenland climate and the Mediterranean hydrology. This indicates that the main climate changes recorded in the North Atlantic are globally in phase with those observed in the Mediterranean region.

Highlights

► We present a high-resolution biochronological records in the Mediterranean Sea. ► Seven biozones are identified basing on the distributional patterns of planktic foraminifera. ► Four bio-events were recognized, and they should improve the chronology of Mediterranean cores. ► A similarity between the global climate and the Mediterranean hydrology is observed.

Keywords : Mediterranean Sea, planktonic foraminifera, SST, LGM, bio-event, AMS14C.

1. Introduction

Since the Mediterranean Sea is located at the interface between the European temperate westerlies and the African subtropical zone, it's considered of great interest to yield information on paleoclimatic and palaeoceanographic changes acting at different time scales during the Late Quaternary (Cacho et al., 1999, 2000; Sierro et al., 2005; Di Donato et al., 2008, 2019; Melki et al., 2009; Sprovieri et al., 2012; Gàmiz et al., 2014 and references therein). The present-day Mediterranean climate is characterized by a strong seasonality of rainfall and temperature with mild and wet winters and warm and dry summers (Quézel and Médail, 2003; Lionello et al., 2006; Bout-Roumazeilles et al., 2013).The northern Mediterranean regions are characterized by mean annual SSTs lower than those presented in the other sub-basins. The lowest values are recorded in the Gulf of Lions (17.3°C), the Northern Adriatic Sea (17.1°C) and the Siculo-Tunisian Strait (19°C) (Locarnini et al., 2019) whereas the Levantine Basin constitutes the warmest region with mean annual SSTs of about 21.6°C.

Several studies based on different marine proxies (stable isotope, calcareous nannoplankton, benthic and planktonic foraminifera, dinoflagellates) have been used in the reconstruction of palaeoceanographic changes in the Mediterranean Sea during the Late Quaternary providing useful insights to define biological events or biozones (Pujol and Vergnaud-Grazzini, 1989; Capotondi and Morigi, 1996; Capotondi et al., 1999; Asioli et al., 2001; Sprovieri et al., 2003; Sbaffi et al., 2001, 2004; Geraga et al., 2005; Di Donato et al., 2008, 2019; Dormoy et al., 2009; Triantaphyllou et al., 2009; Siani et al., 2010; Boussetta et al., 2012; Lirer et al., 2013). Among these, changes in planktonic foraminifera assemblages represent one of the most powerful tools used for paleoclimate and palaeoceanographic reconstructions. Their abundance and distribution in the water masses makes them a reliable proxy of sea-surface temperature (SSTs), salinity and food availability (Pujol and Vergnaug-Grazzini, 1995; Kucera, 2007; Hernández-Almeida et al., 2011; Rigual-Hernández et al., 2012; Mallo et al., 2017; Schiebel and Hemleben, 2017).

Within this context, high-resolution studies carried out in different basins of the Mediterranean Sea emphasized that the distributional pattern of the planktonic foraminiferal assemblages can also be useful for regional correlation during the Late Quaternary as past hydrological and climate variations had a similar impact in this area (i.e., Vergnaud-Grazzini

et al., 1988; Sprovieri et al., 2003; Incarbona et al., 2008; Rouis-Zargouni et al., 2010; Siani et al., 2010; Lirer et al., 2013; Ferraro et al., 2018).

In the present paper, we use changes in the planktonic foraminifera assemblages to define biozones characterizing each of the three selected Mediterranean basins over the last 24 kyr and relate these changes to different hydrological parameters such as temperature, productivity and stratification of the water column. We have selected three deep-sea cores: REC13-53 recovered in the Siculo-Tunisian Strait, KET80-19 from the Tyrrhenian Sea, and MD84-641 in the Levantine Basin respectively (Fig. 1). Our climatic and micropaleontological dataset benefits from an accurate chronological framework based on oxygen stable isotope and radiocarbon dates performed on planktic foraminifera.

2. Materials and Methods

2.1. Study material

Three deep sediment cores are selected for this study and collected in the Tyrrhenian Sea (western basin), the Siculo-Tunisian Strait (central basin), and the Levantine Basin (eastern basin) respectively (Table 1 and Fig. 1).

Core REC13-53 was collected during the RECORD cruise on board the R/V Urania in November 2013 in the Siculo-Tunisian Strait off Pantelleria Island. This core consists of 5 m of grey to brown muddy to muddy-silty layers with intercalation of some volcanic ash layers (tephra).

Core KET80-19 was collected during ETNA80 cruise of the R/V Le Noroit in the Tyrrhenian Sea. This core consists of 6 m of hemipelagic ooze with several centimetric tephra layers (Kallel et al., 1997b; Kallel et al., 2004).

Core MD84-641 was recovered during the NOE cruise of the R/V Marion Dufresne in August 1984. This core presents 11.61 m of pale cream to yellowish brown foraminifera/nannofossil marl ooze with 9 olive green sapropels layers (Calvert et al., 1992). In this study, we only analyzed the first meter of the core covering the last 24 kyr. The sedimentary unit presents a black layer rich in organic carbon between 24 and 40 cm, referred to the sapropel S1 (Fontugne et al., 1989).

2.2. Stable oxygen isotope analyses

Stable oxygen isotopes ($\delta^{18}O$) were measured on planktonic foraminifera at the Laboratoire des Sciences du Climat et de l'Environnement (LSCE) on a GV Isoprime mass spectrometer. Isotopic measurements were obtained for REC13-53 on the planktonic foraminifera *G. bulloides* (250-315 µm fraction), with a sampling resolution every 8 cm along the 5 meters of the core and corresponding to 65 samples. About 4 to 30 shells were sampled for each analysis, cleaned using methanol and ultrasonic bath, and heated at 380 °C during 45 min. The measurements are reported versus the Vienna Pee Dee Belemnite standard (VPDB) with NSB19 standard at $\delta^{18}O$ = - 2.20‰, with a mean external reproducibility (1σ) of carbonate standards of ± 0.05‰.

2.3. Radiocarbon analyses

Thirteen radiocarbon dating were performed on core REC13-53 on monospecific planktonic foraminifera shells of *G. bulloides*, *G. ruber* and *N. incompta* in the size fraction >150µm. Samples were processed according to the procedure described by Tisnérat-Laborde et al. (2001) slightly modified for samples of mass less than 2 mg. Samples were directly introduced in the main branch of Y glass reactor and are leached with only 100 µL of HNO_3 at 10^{-2} M. 10 drops of pure H_3PO_4 were added in the second branch of tube. Then, the reactor is rapidly connected to semi-automated carbonate lines. Samples were transformed by hydrolyse into CO_2 and the released CO_2 is dried, cryogenically transferred into µtubes (3 x 7 mm) and then µtubes were sealed. CO_2 samples (from 70 to 160 µgC) were measured with the gas ion source at *ECHo*MICADAS at the LSCE (Gif-Sur-Yvette, France) using coupling of cracker system to the gas handling system (Wacker et al., 2013; Tisnérat-Laborde et al., 2015). ^{14}C results are reported in conventional age BP according to the convention of Stuiver and Polach (1977), normalized to the base of $\delta^{13}C$ of –25.0‰ relative to the Pee Dee Belemnite (PDB) international standard, and corrected by the age of the background subtraction. One date was measured on UMS-ARTEMIS (Pelletron 3 MV) AMS facilities (CNRS-CEA Saclay, France). The age models for the cores were derived from the calibrated planktonic ages by applying a variable sea-surface reservoir ^{14}C correction (Siani et al., 2000, 2001) and using INTCAL20 (Reimer et al., 2020) calibration curve in the Oxcal 4.4 software (Bronk-Ramsey, 2009).

2.4. Planktonic foraminifera analyses

For micropaleontological analyses, samples were dried at 50°C, washed through mesh diameters of 150 μm using distilled water. Quantitative and qualitative analyses on planktonic foraminifera have been performed on the fraction > 150 μm. This fraction was subsequently divided by a microsplitter into aliquots each containing at least 300 specimens of planktonic foraminifera. All the specimens present in the sub-samples were then counted and identified according to the taxonomic concept adopted by Pujol and Vergnaud-Grazzini (1995) and Schiebel and Hemleben (2017). On the basis of this classification, more than 94% of our planktonic foraminifera fauna is dominated by the following species: *Globigerina bulloides*; the two *Neogloboquadrina* species *N. pachyderma* and *N. incompta* which are referred to left and right coiling forms, respectively; *Globorotalia truncatulinoides* right (r.c) and left (l.c) coiling species; *Globigerinoides ruber* (s.l) including both varieties (pink and white); *Orbulina universa*; *Globorotalia scitula*; *Globorotalia inflata*; *Globigerinita glutinata*; *Turborotalia quinqueloba*; *Globigerinella calida; Globigerinoides conglobatus*; *Globigerinoides sacculifer* (s.l), including *Globigerinoides trilobus* and *Globigerinoides. sacculifer* sensu strictu (s.s).

Then, all the results of planktonic foraminifera counting are presented in terms of their relative abundances (percentages of the total number).

2.5. Modern Analogue Technique (MAT)

We derived Annual SSTs for the three Mediterranean cores by the use of the Modern Analog Technique (MAT, Hutson, 1980; Prell, 1985) through planktonic foraminifera census counts using the Paleoanalog program (Therón et al., 2004). For this study, the MAT statistical temperature reconstructions are based on the recently developed ForCenS foraminiferal database (Siccha and Kucera, 2017). This database consists of synthesis of planktonic foraminifera assemblage counts from surface sediment samples which comprise 4.205 singular counts from unique sites worldwide. The data set includes the compilations of numerous data bases: CLIMAP (CLIMAP Project members, 2009), the Brown University Foraminiferal Database (BUFD) (Prell et al., 1999), the ATL947 database (Pflaumann et al., 2003) and MARGO (Kucera et al., 2005; Hayes et al., 2005). The individual datasets of Hüls et al. (1999), Mohtadi et al. (Mohtadi et al., 2005; Mohtadi, 2010), Salgueiro et al. (2008), Siccha et al. (2017) and Munz et al. (2015) are also considered into the database. However, in

the present study we have considered only the Mediterranean Sea core tops (125 samples) and 632 core tops from the North Atlantic Ocean. We have chosen this dataset as it is the most extensive and most recent compilation to date. It contains more samples in the Atlantic Ocean and has undergone to the process of transparent Quality control. In fact, samples of insufficient quality were flagged and excluded from this database (Siccha and Kucera, 2017).

We used the modern analogue technique (Hutson, 1980; Prell, 1985; Kallel et al., 1997a) to compare fossil planktonic foraminiferal samples to this data base and to identify, for each fossil assemblage, the 10 best modern analogues. The modern analogue approach uses dissimilarity coefficients to measure the mean degree of dissimilarity between each fossil samples and the modern samples of the reference data base. Among the different kinds of dissimilarity coefficients, it has been demonstrated that the "squared chord distances" type, which we use in the present study, gives the best temperature estimates with the smallest standard deviations between the observed and estimated climatic parameters (Prell, 1985) and has the advantage of giving importance even to low percentage planktonic species. For each fossil association of planktonic foraminifera, the SST at which it developed is given by the dissimilarity weighted temperatures of the 10 best modern analogues selected by the statistical analysis. According to Prell (1985), when the dissimilarity coefficient is lower than 0.21, the estimated SSTs are considered as reliable. Annual SSTs are considered in the present study. Finally, for each sample of the reference database, the temperatures were extracted from the World Ocean Atlas (WOA, 1998) at a depth of 0 m.

3. Results and discussion

3.1 Age model

The age model of core REC13-53 is based on oxygen isotope stratigraphy and by 13 AMS ^{14}C measurements carried out on monospecific planktonic foraminifera all along the core (Fig.2). The conventional radiocarbon ages were converted into calendar age using INTCAL20 (Reimer et al., 2020) and the ^{14}C calibration software Oxcal 4.4 (Bronk-Ramsey, 2009; Bronk-Ramsey and Lee, 2013). The calibration integrates a marine reservoir correction (reservoir ^{14}C age) according to Siani et al. (2000, 2001). The calibrated age ranges are reported in calendar years BP and refer to an uncertainty at 2σ (Tab 2). The mean calculated sedimentation rate is estimated at about 22 cm/kyr from the Late Glacial to the Holocene.

As for the two other cores, KET80-19 and the MD84-641 presented above, their age model have already been published by Kallel et al. (1997b, 2004); Fontugne and Calvert (1992) and

Melki et al. (2010), respectively. In this study, we have refined the previous age models by recalibrating the published radiocarbon ages using INTCAL20 (Reimer et al., 2020) (Tab 2).

3.2 Mediterranean paleoclimatic record

3.2.1. High resolution Siculo-Tunisian Strait paleoclimatic record

3.2.1.1. *Oxygen isotope stratigraphy*

Stable oxygen isotopes ($\delta^{18}O$) were analyzed on the planktonic foraminifera species *G. bulloides* (Fig.2, 3) exhibiting a pattern similar to those observed in nearby deep-sea cores (Essallami et al., 2007). The $\delta^{18}O$ record for core REC13-53 displays a glacial to Holocene $\delta^{18}O$ difference of ~ 3.2 ‰. The heaviest $\delta^{18}O$ values (up to ~3.5 ‰) are found from ~23 to ~18 kyr followed by a two-step decreasing deglacial trend reaching 0.7 ‰ at ~8.6 kyr interrupted by centennial to millennial $\delta^{18}O$ variability (~2.8 to 2.5 ‰) from ~16 to 12 kyr (Fig.3). From ~12 to 8.5 kyr, the $\delta^{18}O$ values are marked by a decreasing trend (~1.7 ‰) followed by a short-term variability until ~ 5 kyr. Afterwards, steady $\delta^{18}O$ values at ~ 1 ‰ are recorded until present-day.

3.2.1.2. *Sea-surface temperature (SSTs)*

Over the last 24 kyr, Siculo-Tunisian Annual SST estimates by modern analogue technique (MAT) display large amplitude temperature fluctuations, indicating a succession of cold and warm periods (Fig. 3). Annual SST estimates range from ~9°C during the glacial period (GS-2) to ~19°C for the Holocene. The lowest values are recorded between 19 kyr to 15 kyr and 12.9 kyr to 11.6 kyr since the transition from the Late Glacial (GS-2b) and the Oldest Dryas/Heinrich Event (HE) 1 (GS-2a) and Younger Dryas (GS-1) respectively, whereas the warmest are observed during the Bolling/Allerod (GI-1) (14.8 kyr to 12.9 kyr) and the Holocene period. SST estimates present good dissimilarity coefficients all along the record generally < 0.21 with an average value of 0.13 (varying between 0.05 and 0.24). The mean standard deviation of SST estimates is ~0.69°C during the Holocene and ~1.38°C since the late glacial period (Fig.3). Interestingly, the comparison between SST estimates of core REC13-53 with $\delta^{18}O$ of NGRIP ice core reveal that the main climatic phases observed in the North Atlantic region over the last 24 kyr match well those recorded in the Siculo-Tunisian Strait (Fig.3).Therefore, in the following sections we relate our planktic foraminiferal record

to the NGRIP event stratigraphic framework (Lowe et al., 2008; Blockley et al., 2012; Rasmussen et al., 2014) in order to better identify the relationship between North Atlantic to regional climatic changes and the response of microfaunal assemblages in the Mediterranean basin over the last 24 kyr.

3.2.2. Planktic foraminiferal record over the last 24 kyr in the Mediterranean Sea

The study of the assemblage variations of planktonic foraminifera fauna along the Mediterranean cores permits to define biological events or biozones. These biozones are defined, on the basis of temporary local appearance and/or disappearance of some specific taxa of planktonic foraminifera, or by their noticeable abundance peaks. In this biochronological framework, we will present and discuss our results in comparison with previous studies performed in the main basins of the Mediterranean Sea (Sprovieri et al., 2003; Sbaffi et al., 2001, 2004; Principato et al., 2003; Ceraga et al., 2005; Di Donato et al., 2008; Triantaphyllou et al., 2009).Therefore according to the planktic foraminiferal distributional pattern, we reconstruct the biochronological events of the three deep-sea sediment cores. Here, we identify seven biozones in cores REC13-53 and KET 80-19 and only six biozones in MD84-641 during the last ~24 kyr (Fig. 4) that are summarized here below.

Biozone 7

The biozone 7 (Fig. 4, 5) represents the time interval corresponding to the Late glacial period (GS2-b, c) including the last glacial maximum (LGM). It has been identified in the Siculo-Tunisian Strait by the heaviest $\delta^{18}O$ values dated between 23.2±0.46 and 18.3±0.79 kyr, in the Tyrrhenian Sea from 23.5±0.46 to 18.2±0.58 kyr and in the Levantine basin between 23.4±0.68 and 19±0.64 kyr. SSTs estimates from core REC13-53 (Siculo-Tunisian Strait) are generally low ~10°C, even though marked by a short-term centennial variability of ~3°C between 23.2 to 19.3 kyr (Fig. 5a). The planktic foraminiferal fauna presents a high diversity displayed by a mixture between cold and warm species dominated by *N. incompta*, (40%), *T. quinqueloba* (11%), *G. bulloides* (21%), *G. glutinata* (13%), *G. scitula* (5%) with a peak of about 11% at 18.1±0.8 kyr, and by *G. ruber* (10%). A sudden decrease of the subtropical species *G. ruber* and a coeval peak of the subpolar species *T. quinqueloba* (28%) at 18.3±0.79, mark the upper boundary of this biozone. The two relevant peaks of *G. scitula* and

T. quinqueloba simultaneous to the drop of *G. ruber* were also observed in the core KET80-19, at 18.2±0.58 kyr. The planktic foraminiferal assemblage show a good similarity with that from REC13-53 core whilst SSTs estimates indicate different features with a mean value of 11°C between 23.5-22 kyr and an increase of 3°C until 18 kyr (Fig. 4b, 5c).

The particularity of these two faunal assemblages is the simultaneous presence of both the subtropical species *G. ruber* (up to 13% for KET80-19 and 10% for REC13-53) and the subpolar species *N. incompta* (32% for KET80-19 and 40% for REC13-53) as well as the relative abundance peak of *T. quinqueloba* at ~18.2 kyr that are also observed in the nearby core GNS84-C106 collected at the same latitude in the Gulf of Salerno but at lesser depth on the continental margin (Di Donato et al., 2008). However, the foraminiferal assemblage is slightly different in core GNS84-C106 marked by higher abundances of the subtropical species *G. ruber* (30%) and a lower percentage of the subpolar one *N. incompta* (18%). The low frequency of the latter species was probably due to the low bathymetry of the recovered core at water depth of 293 m off the Sele Plain in the Gulf of Salerno. This location probably prevents the occurrence of the deep dwelling species such as *N. incompta* especially during the late glacial sea-level lowering whereas the abundance of the warm species *G. ruber* is rather related to the adopted mesh sieve. Interestingly, Buccheri et al. (2002) analyzed the same core (GNS84-C106) with lower mesh sieve (>106 µm) and found different percentages (10% for *G. ruber* and 10% of *N. incompta*). In both studies, the percentage of *N. incompta* is lower than that observed in our core, reflecting the shallower depth of the core GNS84-C106 as indicated above. However, the highest percentage of the shallow dwelling taxa *G. ruber* observed in Di Donato et al. (2008) is rather related to the different mesh sieve used in that study (>150 µm) leading to a larger loss of the small size surface dwelling taxa *T. quinqueloba* (60 to 70% in Buccheri et al., (2002) compared to 5-10% in Di Donato et al. (2008)).

In the Levantine basin the assemblage is dominated by the subtropical species *G. ruber* (up to 68%) and the subpolar species *N. incompta* (21%) making it significantly different from that observed in the two other core sites (Fig. 4c).

Based on the stratigraphic subdivision, the identified biozone 7 from our three cores is correlated with the two sub-ecozones 8Fa (GS-2c) and 8Fb (GS-2b) from the ODP hole 963 D (Sprovieri et al., 2003) as well as the biozone 7 from core79-22 located in the Cefalù basin (southern Tyrrhenian Sea; Sbaffi et al., 2001). It also corresponds to the two compositional-

zones F5c and F5b of the core GNS84-C106 located in the Gulf of Salerno (Di Donato et al., 2008) (Fig. 6).

Biozone 6

Biozone 6 corresponds to the first step of the deglaciation as indicated by progressive lighter $\delta^{18}O$ values dated between 18.3±0.79 and 14.8±0.45 kyr in the Siculo-Tunisian Strait (Fig. 3), from 18.2±0.58 to 14.5±0.55 kyr in the Tyrrhenian Sea and between 19±0.64 and 15±0.48 kyr in the Levantine basin respectively. The onset of this biozone is marked by the decline of the subtropical species *G. ruber* in REC13-53 and KET80-19 cores while those from MD84-641 slightly decrease without reaching values less than 60% (Fig. 4a, 4b). The planktic foraminiferal microfauna in core REC13-53 is generally characterized by the predominance of the subpolar species *N. incompta* (38%), and subordinately *G. bulloides* (23%), *T. quinqueloba* (7%), and *G. scitula* (4%). Interestingly, the species *G. glutinata* is also highly representative of this interval with a mean percentage of about 23% whereas, the subtropical species *G. ruber* is almost absent. The first postglacial occurrence of the two species *G. truncatulinoides* r.c and *G. inflata* is observed at 14.6±0.4 and 15.3±0.6 kyr, respectively. These two bio-events occurred as well in core KET80-19 at 14.3±0.45 and 15.1±0.78 kyr, respectively. According to the cold Annual SST estimates (9.5°C in REC13-53 and KET80-19); biozone 6 corresponds to the cold GS-2a event recorded in NGRIP ice core (Fig. 5a, 5c). This cold episode was identified between 17 kyr and 14.7 kyr in the Gulf of Salerno as indicated by a SST decrease of ~8°C (Di Donato et al., 2008). In addition, this cold event was also recorded in the Alboran Sea by alkenone SST reconstructions and attributed to the Heinrich event H1 (Martrat et al., 2014; Hodell et al., 2017).

In the Levantine basin, the microfauna assemblage is rather dominated by the subtropical species *G. ruber* (62%) and by the subpolar species *N. incompta* (26%). However, due to the high dissimilarity coefficient (>0.21), Annual SST estimates during this time-interval have to be considered with caution (Fig. 5e, 5f).

Biozone 6 is tentatively correlated with the sub-biozone 8Fc (GS-2a) of Sprovieri et al. (2003) in the Siculo-Tunisian Strait (Fig. 6), despite the small discrepancy related to the quantitative distribution of *G. glutinata*, more abundant (25%) in our record compared to the nearby ODP site 963 D. It also corresponds to the two sub-zone 6b and 6a of Sbaffi et al. (2001) in the Tyrrhenian Sea as corroborated by deglacial lighter $\delta^{18}O$ values as well as the compositional-zone F5a of Di Donato et al. (2008) considering the disappearance of *G. ruber* and the

predominance of the cold and temperate species *N. incompta*, *G. scitula* and *G. glutinata* respectively.

Biozone 5

Biozone 5 corresponds to the time interval between 14.8±0.45 and 12.9±0.37 kyr in the Siculo-Tunisian Strait, from 14.5±0.55 to 12.9±0.91 kyr in the Tyrrhenian Sea and between 15±0.48 and 13.5±0.35 kyr in the Levantine basin. A prominent Annual SST rise of about 7.5°C marks this biozone in the Siculo-Tunisian Strait and the Tyrrhenian Sea, corresponding to the interstadial Bølling/Allerød/GI-1(Fig. 5a, 5c). However, the aforementioned warming is less pronounced in the Levantine Basin as indicated by the Annual SSTs record (~2°C) (Fig. 5e). The onset of biozone 5 in the two cores REC13-53 and KET80-19 is defined by the re-entry of the warm species *G. ruber* and the occurrence of *G. inflata* as well as of *G. truncatulinoides* r.c and *O. universa* even with low percentages (Fig. 4a, 4b). In addition, in the Siculo-Tunisian Strait, moderate percentages of subpolar and temperate species *N. incompta* and *G. bulloides* (20% and 24%, respectively) marked this biozone even though the latter species is more abundant in the Tyrrhenian Sea reaching 41%. The microfaunal assemblage is also characterized by the noticeable decrease of the colder species *G. scitula* and *T. quinqueloba* as well as by the cosmopolitan species *G. glutinata.* A decline of *G. scitula* is recorded at 14.8±0.45 kyr in core REC13-53 and at 14.3±0.32 kyr in core KET80-19 respectively. This pattern was also observed in the southern Tyrrhenian Sea by Sbaffi et al. (2004) and in the Gulf of Salerno by Di Donato et al. (2008). Two colder SST spells marked by the coeval decrease of *G. ruber* and the rise of *N. incompta*, are observed in the Siculo-Tunisian Strait at ~14.4±0.35 and ~13.4±0.40 kyr. These short-term events can be attributed, taking into account the age model uncertainties at 2σ, to the GI-1d and GI-1b events respectively, described in Greenland ice cores and according to the extended INTIMATE stratigraphy (Rasmussen et al., 2014). The two falls of *G. ruber* were already reported in the nearby ODP hole 963D (Sprovieri et al., 2003) as well as in the central and southern Adriatic and Tyrrhenian seas (Asioli et al., 1999, 2001; Siani et al., 2010) and equally related to the GI-1d and GI-1b events.

In the Levantine basin, despite not having occurred significant changes in the faunal assemblage, the onset of the biozone 5 is rather marked by the first occurrence of the species

G. truncatulinoides r.c at 14.5±0.43 kyr and by the increase in abundance of *G. inflata*. As mentioned above, Annual SST estimates indicate a slight increase of about 2°C (Fig. 4c, 5e).

Through these results, we correlate biozone 5 with ecozone 7F (GI-1) of ODP site 963 D (Sprovieri et al., 2003) also characterized by a lower percentage of *T. quinqueloba* and a higher abundance of *N. incompta*, *G. ruber* and *G. inflata*. This biozone is also correlated with the biozone 5 of Sbaffi et al. (2001, 2004) (Fig. 6) marked by a greater abundance of *G. ruber* and a lower abundance of *G. glutinata* and displaying two consecutive peaks of *G. inflata* and with the lower part of the compositional-zone F4 proposed by Di Donato et al. (2008). Moreover, based on the inferred age models, biozone 5 also corresponds to biozone 5 of the core C69 in the southern Aegean Sea (Geraga et al., 2005) and to ecozone APFE-9 (14-13.1 kyr) of the core NS-14 in the south-eastern Aegean Sea (Triantaphyllou et al., 2009) (Fig. 6).

Biozone 4

Biozone 4 has been identified in the Siculo-Tunisian Strait between 12.9±0.37 and 11.6±0.31 kyr, in the Tyrrhenian Sea from 12.9±0.91 to 11.6±0.33 kyr and in the Levantine basin between 13.5±0.35 and 11.6±0.43 kyr. It corresponds to the Younger Dryas/GS-1 cold event when Annual SST estimates decrease by about 7.5°C and 9.5°C in the REC13-53 and KET80-19 respectively, marking the return to full glacial conditions (Fig. 5a, 5c). The abrupt decrease of the subtropical species *G. ruber* in the three cores permits to define the lower boundary of this biozone. The microfaunal assemblage from core REC13-53 characterizing this interval is marked by the increase in the abundance of cold species *N. incompta* (38%) with a relevant peak (up to 55%) at 12.8 kyr and of *T. quinqueloba* (12%), accompanied by the presence of *G. glutinata* (12%) and *G. bulloides* (21%). The assemblage is also characterized by the near disappearance of *G. ruber* even though a slight increase is observed at ~12.3 kyr. While showing a large resemblance with core REC13-53, the planktic assemblage from core KET80-19 slightly differs in the abundance of the two species *N. incompta* and *G. glutinata* reaching 22 and 35%, respectively. A similar planktic foraminiferal assemblage to core KET80-19 is observed in the nearby core GNS84-C106 (Di Donato et al., 2008). However, a marked difference concerns the significant presence of the subtropical species *G. ruber* (10%), which is not present in our record. As indicated above, the highest frequency of the shallow dwelling taxa *G. ruber* observed in Di Donato et al. (2008) is related to the different

mesh sieve used in that study (>150 µm) leaded to a large loss of the surface dwelling taxa *T. quinqueloba.*

The YD cold event recorded in the Tyrrhenian Sea is also observed in other Mediterranean basins with April-May SST estimates decrease by about 6.5°C in the Siculo-Tunisian Strait (Essallami et al., 2007), ~4°C in the South Adriatic Sea (Siani et al., 2010) and ~4.5°C in the Gulf of Lions (Melki et al., 2009). Our SST estimates in core MD84-641 also show a slight decrease of ~2.5°C during the same time interval (Fig. 5e). This cooling is accompanied by a slight decrease of the warm species *G. ruber*, together with the sudden drop of the subpolar species *N. incompta*. However, a rise in *G. bulloides* is observed from 13.5 kyr with a peak (26%) just at the lower zonal boundary of this biozone. The planktic foraminiferal assemblage is mainly represented by two species of *G. ruber* (65%) and *G. bulloides* (17%) and punctuated by the disappearance of *G. scitula*.

Biozone 4 is correlated with the ecozone 6F (GS-1) of Sprovieri et al. (2003) (Fig. 6) although G. *ruber* and *G. glutinata* are almost absent and *T. quinqueloba* is more abundant. These discrepancies could be explained by the difference between the mesh-size of the sieve adopted in our study (150 µm) and the one (125 µm) used by Sprovieri et al. (2003). In fact, larger sieve meshes lead to a major loss of small sized species such as *T. quinqueloba.* Moreover, this biozone also corresponds to the biozone 4 of Sbaffi et al. (2001, 2004) characterized by a drop in the abundance of *G. ruber* and *G. inflata* and an increase of *G. glutinata* with a peak at 12.3 kyr, and with the upper part of the zone F4 of Di Donato et al. (2008). On the other hand, the biozone 5/4 boundary of MD84-641 is correlated with the biozone 5/4 boundary of Geraga et al. (2005) in the southern Aegean Sea and with ecozone APFE-9/APFE-8 boundary of core NS-14 in the south-eastern Aegean Sea as indicated by an important increase in *G. bulloides* (Triantaphyllou et al., 2009) (Fig. 6).

Biozone 3

Biozone 3 marks the onset of the Holocene as characterized by a consistent lowering of the $\delta^{18}O$ values (Fig.3) covering the time interval between 11.6±0.31 to 9.5±0.14 kyr in the Siculo-Tunisian Strait, 11.6±0.33 to 9.5±0.24 kyr in the Tyrrhenian Sea and from 11.6±0.43 to 9.5±0.29 kyr in the Levantine basin respectively. Annual SST estimates increased again and reached higher values with a large amplitude change of about 7.5 and 8.5°C indicating the end of glacial conditions in the two studied cores REC13-53 and KET80-19 respectively (Fig. 5a, 5c). In accordance with chronology and the climatic feature, this interval corresponds to

the upper part of the Early Holocene (11.6 - 8.2 kyr after Walker et al., 2018). In fact, the re-occurrence of the warmer species *G. ruber*, associated with the marked decrease of the subpolar species *N. incompta*, define the onset of this biozone at about 11.6 kyr (Fig. 4a, 4b). Biozone 3 is characterized by the predominance of *G. ruber* (38%), *G. bulloides* (24%), *G. inflata* (18%), and *G. truncatulinoides* l.c (8%) and by a sudden drop of subpolar species *N. incompta* and by the re-entry of *O. universa*, *G. calida*, and *G. sacculifer* group from 11±0.34 kyr. Interestingly, a significant rise in *G. inflata* is observed in both cores between 11 to 9.5 kyr and culminating with a peak (38%) at 10.3 kyr. A similar increase in *G. inflata* was previously recognized in the northern Tyrrhenian Sea (Carboni et al., 2005), in the Gulf of Salerno (Di Donato et al., 2008), in the south Tyrrhenian Sea (Sbaffi et al., 2004) as well as in the south Adriatic sea (Rohling et al., 1997; Siani et al., 2010), and from several eastern Mediterranean cores (Principato et al., 2003; Geraga et al., 2005), suggesting a strong vertical mixing of the water column and cool environments with relatively eutrophic waters.

In the Levantine basin, the onset of this biozone is especially characterized by the first entry of the subtropical species *G. sacculifer* group (up to 27%) and *G. calida* (4%), and the synchronous disappearance of *N. incompta* (Fig. 4c). Moreover, the last occurrence of *G. truncatulinoides* species with low percentage (4%) is also observed at 10.6 kyr. This biozone is also marked by the strongest presence of *G. ruber* reaching 70% of the total assemblage.

Biozone 3 is correlated with the biozone 5F of Sprovieri et al. (2003), displaying the two coeval major peaks of *G. ruber* at ~11.2 and ~9.7 kyr and the peak of *G. inflata* at ~10.6 kyr, respectively. It also corresponds to the biozone 3 of Sbaffi et al. (2001, 2004) as also corroborated by a coeval lowering of the planktic foraminifera $\delta^{18}O$ values in the south Tyrrhenian Sea and compositional-zone F3 of Di Donato et al. (2008) (Fig. 6) equally characterized by the reoccurrence of *G. ruber* and the decrease of *N. incompta*.

Biozone 2

Biozone 2 is identified between 9.5±0.14 and 5.6±0.34 kyr in the Siculo-Tunisian Strait, from 9.5±0.24 to 5.6±0.21 kyr in the Tyrrhenian Sea and between 9.5±0.29 to 4.5±0.27 kyr in the Levantine basin. This biozone is related to the interval between the end of the Early Holocene and the middle Holocene including the sapropel S1 deposition in the Eastern Mediterranean Sea (De Lange et al., 2008). In our records, the sapropel S1 was only observed in core MD84-641 and deposited between 9.3 and 6.7 kyr during the most recent period of stagnation in the

Eastern Mediterranean (Rossignol-Strick et al., 1982; Rohling, 1994; Fontugne et al., 1994; Kallel et al., 1997a; Mercone et al., 2000).

A marked increase of the subpolar species *N. incompta* (25%) marks the base of this biozone in core REC13-53, even though SST estimates indicate almost constant values (19.5°C) throughout the entire interval. The dominant species are represented by *G. inflata* (19%), *G. ruber* (33%) and *G. bulloides* (20%). The warm species *O. universa*, *G. calida*, *G. sacculifer* group, are also present within this interval even though with low percentages. The assemblage characterizing this biozone is slightly different to that observed in the Tyrrhenian Sea core KET80-19 where the abundance of the species *G. inflata* is of 15%, 22% for *G. ruber* and 11% for *G. bulloides*. However, the subpolar planktic foraminifera *N. incompta* (45%) is more abundant, exhibiting an outstanding peak of 66% at 6.8±0.15 kyr, that could explain the SST decrease by about 3.5°C in this core. The planktic faunal assemblage characterizing this biozone is slightly different from that recorded in the continental shelf (i.e. core GNS84-C106; Di Donato et al., 2008), which is characterized by lower abundances of the subpolar deep-dwelling species *N. incompta* (13%) and higher percentages of the subtropical species *G. ruber* (35%). These differences are likely related to the low bathymetry of the GNS84-C106 core. The decrease in SST (between 9.5 and 5.6 kyr) is also observed in the southern Tyrrhenian Sea (Sbaffi et al., 2001) but less pronounced than that recorded in core KET80-19, in the Gulf of Lion (Melki et al., 2009) and in South Adriatic Sea (Siani et al., 2010). However, this cooling period is not recorded in GNS84-C106 core (Di Donato et al., 2008), once again related to the low depth of the collected core which would record a greater development of planktic superficial forms.

The onset of biozone 2 in the Levantine basin is characterized by an increase of *N. incompta* and by a drop of *G. truncatulinoides* (l.c) as well as by a significant increase of *G. ruber* (more than 90%) followed by the disappearance of *G. inflata*, *G. sacculifer* group and *G. truncatulinoides* l.c. From 8 kyr, the two species *G. sacculifer* group and *G. inflata* reappear again reaching 26 and 9% at 7.4±0.198 and 5.8±0.245 kyr respectively (Fig. 4c). The planktic foraminifera assemblage characterizing this biozone indicate the onset of enhanced water column stratification in the eastern Mediterranean basin during the S1 deposition. The peak of *G. inflata* observed after the end S1 is correlated with that recorded by Geraga et al. (2005) and Triantaphyllou et al. (2009) in the south-eastern Aegean Sea suggesting the return of deep water ventilation and the onset of the modern circulation regime in the Levantine Basin.

Biozone 2 is correlated with the ecozone 4F and the lower part of the ecozone 3F of Sprovieri et al. (2003) in the Siculo-Tunisian Strait (Fig. 6), even though a higher percentage of *G. inflata* is observed in our record. On the basis of the planktic foraminiferal species, biozone 2 is also correlated to the biozone 2 of Sbaffi et al. (2001, 2004) and with the compositional-zone F2 of Di Donato et al. (2008) (Fig. 6).

Biozone 1

Biozone 1 corresponds to the time interval between 5.6±0.34 and 0.4±0.10 kyr in the Siculo-Tunisian Strait, from 5.6±0.21 to 1.3±0.08 kyr in the Tyrrhenian Sea. This interval covers the upper interval of the middle Holocene and the whole period of the upper Holocene (the last 4.2 kyr). The onset of this biozone is marked by the reoccurrence of *G. truncatulinoides* r.c species (Fig. 4a, 4b). In core REC13-53, no remarkable Annual SST changes can be observed since 5.6 kyr, with mean values around 19°C similar to those observed today. The planktic foraminifera assemblage is dominated by *G. bulloides* (25%) and *G. inflata* (around 30% with a peak of about 43% at 5.3 kyr) and by the subtropical species *G. ruber* (26%).The warmer species, including *G. sacculifer* group, *G. rubra* and *O. universa* also characterize this biozone even if with low percentages. The subpolar species *N. incompta* is present with moderate percentage of about 15% in the lower boundary and starts to decline at about 4 kyr before disappearing. *G. truncatulinoides* reaches its highest abundances (up to 10%) with right coiling forms in the lower part between 4.3 and 2.3 kyr and left coiling forms in the middle and upper part of this interval from 4.1 kyr. Indeed, the re-occurrence of this species at 5.6 kyr has been previously recorded by Sbaffi et al. (2001, 2004) even though the inferred chronology indicates for this bio event and older age (6.5 kyr) compared to our record. This phase shifts between the Tyrrhenian Sea cores (KET80-19, BS79-22, and BS79-38) could be due to a discrepancy in the age models, indeed in core KET80-19, the inferred bioevent is well constrained between two ^{14}C dated control points, whereas in both cores BS79-22 and BS79-38, the age model was rather based on the correlation of some regional Holocene cooling events observed in core MD95-2043 recovered far in the Alboran Sea (Cacho et al., 1999).

Biozone 1 is correlated respectively with the upper part of the ecozone 3F (marked by the reoccurrence of *G. truncatulinoides)*, ecozone 2F and 1F of Sprovieri et al. (2003), with the biozone 1 of Sbaffi et al. (2001, 2004) and with the two compositional-zone F1b and F1a of Di Donato et al. (2008) (Fig. 6) indicated also by the reoccurrence of *G. truncatulinoides*.

3.3 Factors controlling the biochronological events in the Mediterranean Sea

In this study, in order to define biozones and/or biochronological events, we have compared the micropaleontological and climatic reconstructions ($\delta^{18}O$ and SST) obtained from three sediment cores recovered from the Siculo-Tunisian Strait, the Tyrrhenian Sea and the Levantine Basin and relate the changes in planktic foraminifera to different hydrological parameters such as temperature, productivity as well as water column stratification. The quantitative planktic foraminiferal distribution patterns, the succession of the biozones and the climatic records are reported in Fig. 4 and 5.

Throughout these records, we have identified seven biozones in the western and central basins and six in the eastern Mediterranean basin during the last 24 kyr. We used the abundance variations of some planktic foraminiferal species living at different depths of the water column to interpret the palaeoceanographic changes along the sediment cores and to define the boundary of the different biozones.

A notable consistency is observed between the faunal record from the Siculo-Tunisian Strait and the Tyrrhenian Sea (Fig. 4 and 5). In fact, the abundance of the colder species in the biozone 7 allows us to deduce that cold and productive waters occupied both the Siculo-Tunisian Strait (Sprovieri et al., 2003) and the Tyrrhenian Sea (Sbaffi et al., 2001) at that time interval. In addition to the presence of the subpolar species (i.e. *N. incompta* and *G. scitula*), *T. quinqueloba* is also abundant with a peak at around 18.2 kyr considering the uncertainties in the age models recorded in both basins. Former studies in the Mediterranean Sea reported that high percentage of *T. quinqueloba*, that thrives in cool surface waters (Rohling et al., 1997), is linked to high surface water productivity (Pujol and Vergnaud-Grazzini, 1995; Sprovieri et al., 2003), whereas the abundance of *N. incompta* is related to the presence of deep chlorophyll maximum (DCM) (Rohling and Gieskes, 1989; Sprovieri et al., 2003). The high abundance of *G. scitula* in these records should also reflect, during the late glacial period, enhanced vertical mixing which leads to enhanced eutrophic condition in the surface water masses (Rogerson et al., 2004).

The LGM-Holocene temperature gradient of ~5.5°C recorded in the Siculo-Tunisian Strait and Tyrrhenian Sea, is in agreement with reconstructed SST in the central and the western Mediterranean Sea (Sbaffi et al., 2001; Hayes et al., 2005; Essallami et al., 2007). This scenario is however different in core MD84-641 where SST difference between LGM and

Holocene is only ~ 2.5°C most likely due to the high dissimilarity coefficients associated to the glacial SST estimates in this region, which make the inferred SST not very representative (Fig. 5e, 5f). Indeed, the weak late glacial cooling was also reported in the eastern Mediterranean Sea by a previous study using artificial neural network (ANN) applied to planktic foraminiferal counts (Hayes et al., 2005).

During the Oldest Dryas/GS-2a climatic event (Biozone 6; Fig. 5a, 5c), Annual SSTs are colder than the Holocene period by ~ 9.5°C in the Siculo-Tunisian Strait and Tyrrhenian Sea.In fact, this cold period is associated with the disappearance of warm fauna and by the presence of the subpolar species *N. incompta*, *G. scitula*, and *T. quinqueloba*. This interval was previously identified in the Tyrrhenian Sea (Di Donato et al., 2008) and also well correlated with SSTs cooling by Uk_{37} alkenones reconstructions recorded in the Alboran Sea, corresponding to the Heinrich event H1 (Martrat et al., 2014; Hodell et al., 2017).

The onset of the post glacial warming, dated at ~14.8±0.45 kyr in the Siculo-Tunisian Strait and at ~14.5±0.55 kyr in the Tyrrhenian sea records, is characterized by an abrupt increase in Annual SST (7.5°C warmer than the glacial period) (Biozone 5; Fig. 5a, 5c). This episode, attributed to the Bolling/Allerod/GI-1, is equally synchronously recognized in the South Adriatic (Siani et al., 2010), Ionian (Geraga et al., 2008) and Aegean Sea (Triantaphyllou et al., 2009). In the Siculo-Tunisian Strait record, we distinguish three warming episodes corresponding to three abundance peaks of *G. ruber*, interrupted by two short colder events indicated by a slight increase in the abundance of *N. incompta*. Based on the ice-core stratigraphy proposed by Rasmussen et al. (2014), the five episodes defined in the GI-1 period correspond to the Bølling/GI-1e, Older Dryas/GI-1d, Allerød/GI-1c, Intra Allerød/GI-1b and Allerød/GI-1a respectively match well the Annual SSTs variations in core REC13-53. In addition, the first occurrence of the transitional species *G. truncatulinoides*, even with low percentage, and the abundance of *G. inflata* at the base of this interval, suggests the presence of well-mixed water column during winter (Sprovieri et al., 2003), accompanied by relatively eutrophic waters (Pujol and Vergnaud-Grazzini, 1995). The occurrence of *G. inflata* and *G. truncatulinoides*, was also recorded in the Levantine Basin at 15 kyr, demonstrating the presence of deep winter mixed layer. Indeed, *G. inflata* is considered as a species related to cool environment with relatively eutrophic conditions (Pujol and Vegnaud-Grazzini, 1995; Rigual-Hernández et al., 2012; Mallo et al., 2017) and *G. truncatulinoides* is a deep dwelling species (Hemleben et al., 1989; Rigual-Hernández et al., 2012), which reproduces in winter near to the surface and continues to grow at greater depths (Tolderlund and Bé, 1971; Rohling

et al., 1993). The first post glacial occurrence of *G. inflata* in the Mediterranean Sea at around 15 kyr was also documented by previous studies in the Tyrrhenian Sea and the South Adriatic Basin (Jorissen et al., 1993; Capotondi et al., 1999; Sbaffi et al., 2001; Sprovieri et al., 2003; Di Donato et al., 2008; Siani et al., 2010).

The drastic drop in Annual SST (9.5 and 7.5°C in the Siculo-Tunisian Strait and Tyrrhenian Sea, respectively) and the micropaleontological features prevailing during the Biozone 4 indicate a strong cold phase (Fig. 5a, 5c) at the time of the Younger Dryas/GS-1 event. The onset of this biozone is marked by the strong increase of the subpolar species *N. incompta*, in response to this cooling event recorded both in the Siculo-Tunisian Strait and the Tyrrhenian Basin. This species is considered as a deep dweller (Fairbanks and Wiebe, 1980) which reproduces on a synodic cycle (Schiebel and Hemleben, 2005) and that could well live at or below the thermocline (Bé, 1960; 1977; Rigual-Hernández et al., 2012). According to previous Mediterranean studies (Rohling et al., 1997; Sprovieri et al., 2003; Carboni et al., 2005; Siani et al., 2010; Di Donato et al., 2019), the abundance of the *N. incompta*, indicates the development of a DCM. Even in the Levantine Basin, the fauna composition is marked by a slight reduction in the contribution of *G. ruber*, which rather indicates a decrease in the SST estimates in this region (Fig.4c, 5e), while the increase of *G. bulloides*, suggests an enhanced surface primary productivity (Pujol and Vergnaud-Grazzini, 1995; Lirer et al., 2013) in this oligotrophic basin. The cooling phase was also observed in the nearby core MD84-632, from SST estimated by MAT (Essallami et al., 2007). So, the effect of the Younger Dryas climatic change originated from the North Atlantic region was still sensitive as far as the Eastern Mediterranean area (Almogi-Labin et al., 2009; Revel et al., 2010; Mojtahid et al., 2015).

The onset of the Holocene, with the biozone 3 is characterized by the warmer taxa *G. ruber*, associated with high Annual SSTs (~19.5°C) (Fig.4a, 4b, and 5a, 5c). The abundance of the non-spinose species *G. inflata*, the reappearance of *G. truncatulinoides* synchronous with the decline of *N. incompta* in the lower part of this interval recorded both in the Siculo-Tunisian Strait and the Tyrrhenian Basin indicates a strong vertical mixing of the water column during winter (Pujol and Vergnaud-Grazzini, 1995; Rohling et al., 1997; Sprovieri et al., 2003). In fact, the lower abundance of *N. incompta* during this interval preceding the deposition of Sapropel S1, indicates a deep pycnocline between the LIW and the MAW that prevents the development of DCM (Rohling and Gieskes, 1989).

Biozone 2, corresponding to the upper part of the Early Holocene and the middle Holocene until ~5.6 kyr, is marked by a SST drop of ~3.5°C in the Tyrrhenian Sea (Fig. 5c). The SST decrease occurs in two steps from 9.5 to 8.2 and 7.9 to 5.6 kyr respectively. This cooling phase was also recorded in the southern Tyrrhenian Sea by Sbaffi et al. (2001), in the Gulf of Lion by Melki et al. (2009) and in the South Adriatic Sea by Siani et al. (2010). However, such cooling was not recorded in the Gulf of Salerno (Di Donato et al., 2008). This is probably attributed, as indicated in section 3.2, to the difference between the faunal assemblages of the shallow water core GNS84-C106 when compared to those from deeper Mediterranean basins.

This cooling period recorded in the western Mediterranean during the biozone 2, and in part coeval with the deposition of the Sapropel S1 in the Eastern Mediterranean basin, was characterized by a consistent change in the composition of the faunal assemblage marked by the increase of the subpolar species *N. incompta*. In addition, the simultaneous presence of *G. inflata* and *N. incompta* could indicate a period of cooling and/or an intensified contrast in seasonal conditions. In fact, since *N. incompta* is mainly found in association with DCM at the base of eutrophic layer, its higher abundance would suggest stratified waters with euphotic layer (Pujol and Vergnaud-Grazzini, 1989, Rohling et al., 1997; Sbaffi et al., 2001). Sbaffi et al. (2001) reported two short-term Uk'_{37} derived SST cooling (labelled C4 and C3) centered at 8 and 5.5 cal kyr BP respectively. This cooling (3.5-4°C with respect to the Holocene average) related to the high frequency of *N. incompta* is also recorded by using MAT estimates (Sbaffi et al., 2001). Several studies carried out in the Mediterranean Sea show a similar cooling recorded in the Adriatic Sea at 8.2 kyr and between 7.3 to 6.1 kyr (Siani et al., 2010) and in the Gulf of Lions since 9.9 kyr (Melki et al., 2009). This Holocene cooling pattern is also corroborated by pollen data from Aegean Sea cores showing a temperature decrease by about 3°C at ~7 and ~4.7 kyr respectively (Kotthoff et al., 2008). Conversely, our SST estimates in the Siculo-Tunisian Strait does not indicate a Middle Holocene cooling trend. Essallami et al. (2007) display however, two short and lesser cooling events in the Siculo-Tunisian Strait at about 8.5 kyr and 7 kyr. Although $\delta^{18}O$ data from Greenland ice cores (NGRIP, GISP2) do not show apparent cooling during this period except for the short event at ~8.2 kyr, a reconstructed Greenland temperature in GISP2 ice core using argon and nitrogen isotopes exhibits a similar cooling trend to those observed in the central Mediterranean Sea (Kobashi et al., 2017). Moreover, recent findings on the Greenland and Laurentide past ice sheet dynamic show short-term glacier re-advance centered at ~10.4 kyr,

~9.1 kyr, ~8.1 kyr, and ~7.3 kyr respectively, indicative of regional abrupt cooling (Young et al., 2020). Hence, the most plausible feedback mechanism at the origin of such cooling phases could be related to a southward displacement of the polar front in the Mediterranean region initially affecting the Gulf of Lions since about 9.9 kyr and later the central part of the Tyrrhenian Sea. Either, the SST cooling, recorded in the Middle Holocene in the Aegean (Kotthoff et al., 2008) and Adriatic sea (Siani et al., 2010) was attributed to the enhanced intensity of northerly air outbreaks from the Siberian high during winter and spring (Rohling et al., 2002). These cold and dry winter winds lead to buoyancy loss which is at the origin of the recovery of deep-water formation in both North Aegean and South Adriatic seas just after the sapropel S1 (Kotthoff et al., 2008; Siani et al., 2013).

In the Levantine Basin, the distinct disappearance of the deep dwelling foraminifer species *G. inflata* and *G. truncatulinoides* in the biozone 2 (9.5-4.5 kyr) (Fig. 4c), seems likely to be in response to the stagnation conditions related to the cessation of the water column mixing and to the limited horizontal exchange of the water masses between the eastern and western basin. In contrast to the southern Adriatic Sea (Siani et al., 2010), *G. inflata* does not reappear in the core MD84-641 at the time corresponding to S1 interruption between 8.3 and 8.1 kyr (Siani et al., 2010). This could also be due to the low sedimentation rate of this core particularly during S1 that would preclude the tracking of this short-term cooling. Moreover, the water mass stratification was likely related to increased biological productivity resulting from increased nutrient supply and to enhanced Nile river discharge and precipitation over the Mediterranean Sea (Kallel et al., 1997a, 1997b; De Lange et al., 2008; Mojtahid et al., 2015). Therefore, the eastern Mediterranean Sea seems to be characterized by slightly different oceanographic conditions from those occurred in the Tyrrhenian and the Siculo-Tunisian Strait records during the S1 interval.

During the biozone 1 interval corresponding to the upper part of the middle Holocene and the Upper Holocene, Annual SST estimates increase again and reach the same values (19°C) as those recorded at the beginning of the Holocene (Fig. 5a, 5c). The presence of *G. inflata* and the reoccurrence of *G. truncatulinoides* at the onset of this interval starting from 5.6 kyr in the Tyrrhenian Sea and the Siculo-Tunisian Strait confirms the end of water stratification conditions and the establishment of vertical mixing and water convection during winter, as for the modern Tyrrhenian Sea (Pujol and Vergnaud-Grazzini, 1995; Rohling et al., 1997; Carboni et al., 2005).

Our study on the abundance record of planktic foraminiferal species has displayed synchronous fluctuations, within age uncertainties at 2σ, at a regional scale even though some diachronisms have been observed. These findings allow us to identify four biochronological events (bio-events) which can be used as tie-points to establish or to improve the chronology of Mediterranean deep-sea cores. The first bio-event is relative to the peak of *T. quinqueloba* dated at 18.3±0.79 and 18.2±0.58 kyr in the Siculo-Tunisian Strait and the Tyrrhenian Sea, respectively. This bio-event was previously recorded at ~18 kyr in the southern Tyrrhenian Sea (Sbaffi et al., 2001), in the Gulf of Salerno (Di Donato et al., 2008) and in the Siculo-Tunisian Strait (Essallami et al., 2007; Rouis-Zargouni et al., 2010). The second bio-event corresponds to the first postglacial occurrence of *G. inflata* dated at 15.3±0.6 kyr, in the Siculo-Tunisian Strait and 15.1±0.78 kyr in the Tyrrhenian Sea and at 15.6±0.53 kyr in the Levantine Basin. This event was identified by Sprovieri et al. (2003) in the Siculo-Tunisian Strait, by Sbaffi et al. (2001, 2004) and Di Donato et al. (2008) at ~15.2 kyr in the Tyrrhenian Sea. The last postglacial disappearance of the subpolar species *G.scitula* at 14.3±0.32 kyr (Neapolitan Yellow Tuff tephra layer dated by ^{14}C) in the Tyrrhenian Sea and at 14.58 ± 0.32 kyr in the central basin indicates the third bio-event (Last Common postglacial Disappearance (LCD)). This event is also recorded in other well dated core of the Siculo-Tunisian Strait at ~14 kyr (Essallami et al., 2007; Rouis-Zargouni et al., 2010). This bio-event corresponding to LCD of *G. scitula* has been previously reported by several study carried out in the different basins od the Mediterranean (Sbaffi et al., 2001, 2004; Minisini et al., 2007; Di Donato et al., 2008; Melki et al., 2009; Siani et al., 2010). In the Levantine Basin, this event is however observed at 13.6±0.36 kyr despite being well constrained by ^{14}C pointers.

The latest bio-event corresponds to the reoccurrence of *G. truncatulinoides* r.c in the upper part of the Middle Holocene at 5.6±0.34 and 5.6±0.21 kyr in the central and the western basins respectively. This event was previously identified at 5.5±0.34 in the eastern Tyrrhenian Sea (Lirer et al., 2013), in the Gulf of Salerno (Di Donato et al., 2008) and in the Sicily channel (Minisini et al., 2007).

Results from the central basin presents a striking similarity with those obtained in the western basin in terms of planktic foraminiferal assemblages and of biochronological events (Fig. 6). However, minor differences in timing of the different bio-events and boundaries may be related to the available radiocarbon dataset but in general they can be considered synchronous considering the 2σ uncertainty. This finding suggests that these records reflect coeval responses to Mediterranean wide changes in sea-surface temperature and hydrology.

4. Conclusions

We performed a high-resolution micropaleontological study to generate accurate climate and biochronological records along well dated deep sea cores recovered in three major basins of the Mediterranean Sea (the Siculo-Tunisian Strait, the Tyrrhenian Sea and the Levantine Basin). Quantitative variations of fossil planktic foraminiferal assemblages reconstructed along these three cores, covering the last 24 kyr, have permitted to identify seven successive biozones. Our results display that major changes in planktic foraminiferal assemblages have a similar pattern in the central and western basins unlike that of the Levantine Basin.

The comparison of our SSTs estimates and foraminiferal records with those of NGRIP ice-core shows a similarity between the Greenland climate and the Mediterranean hydrology. This indicates that the main climate changes recorded in the North Atlantic are globally in phase with those observed in the Mediterranean region.

Abundance records of planktonic foraminifera display synchronous fluctuations at a regional scale. Four bio-events were hence identified during the last 24 kyr that can be used to establish or to improve the chronology of Mediterranean deep sea cores: i) the peak of *T. quinqueloba* at 18.3±0.79 and 18.2±0.58 kyr in the Siculo-Tunisian Strait and in the Tyrrhenian Sea respectively, ii) the first postglacial appearance of *G. inflata* dated at 15.3±0.6 kyr in the Siculo-Tunisian Strait, 15.1±0.78 kyr in the Tyrrhenian Sea and and at 15.6±0.53 kyr in the Levantine Basin, iii) the postglacial disappearance of the subpolar species *G. scitula* at 14.3±0.32 kyr in the western basin and at 14.58±0.32 kyr in the central basin (Last Common postglacial Disappearance) but at 13.6±0.36 kyr in the Levantine Basin and iiii) the reoccurrence of *G. truncatulinoides* r.c recorded at 5.6±0.34 and 5.6±0.21 kyr in the central and western basin respectively. Some observed differences may be due to the ^{14}C dating uncertainties during some time intervals. They can be used to establish or to improve the chronology of Mediterranean deep-sea cores.

These results provide an improvement and extension of previous climatic and biochronological events elaborated in the different basins of the Mediterranean Sea, facilitating climatic and microfaunal correlations at regional and global scale over the last 24 kyr.

Acknowledgements

We are grateful to Ministry of Higher Education and Scientific research of Tunisia and "Ecole doctorale Sciences Fondamentales de la Faculté des Sciences de Sfax" for financial support. We would like to thank the direction of international relations of the Paris-Sud Paris Saclay University for its Support. This work was financially supported by the French-Tunisian Joint Project PHC-Utique (Partenariats Hubert Curien: N° 14G1002). Financial support was also provided by the French INSU PALMEDS project. We thank the URANIA officers and crew for support and organization of the coring cruise in 2013. The ARTEMIS program is thanked for providing ^{14}C from the Accelerator Mass Spectrometer. The authors would also to thank two anonymous reviewers, and the editor Xavier Crosta for their constructive and stimulating reviews that deeply improved the manuscript.

Credit author statement:

Sonda Zouari has performed the foraminiferal counting and $\delta^{18}O$ analyses.

Giuseppe Siani, Nadine Tisnérat-Laborde and François Thil have performed the radiocarbon analyses.

Sonda Zouari prepared the paper with contributions from all co-authors (Soumaya Boussetta, Giuseppe Siani, Nadine Tisnérat-Laborde and Nejib Kallel).

Elisabeth Michel contribute in the temperatures reconstruction with the new database (forcens)

Abdelaziz Kallel helped us to respond to the reviewer 1 concerning the validation of the our new reconstruction

Declaration of interests

The authors declare that they have no known competing financial interests or personal relationships that could have appeared to influence the work reported in this paper.

Supplementary data

Supplementary material

References

Almogi-Labin, A., Bar-Matthews, M., Shriki, D., Kolosovsky, E., Paterne, M., Schilman, B., Ayalon, A., Aizenshtat, Z., Matthews, A., 2009. Climatic variability during the last ~90 ka of the southern and northern Levantine Basin as evident from marine records and speleothems. Quat. Sci. Rev. 28, 2882–2890. https://doi.org/10.1016/j.quascirev.2009.07.017

Asioli, A., Trincardi, F., Lowe, J.J., Oldfield, F., 1999. Short-term climate changes during the Last Glacial – Holocene transition: comparison between Mediterranean records and the GRIP event stratigraphy. J. Quat. Sci. 14, 373–381. https://doi.org/CCC 0267-8179/99/040373–09$17.50

Asioli, A., Trincardi, F., Lowe, J.J., Ariztegui, D., Langone, L., Oldfield, F., 2001. Sub-millennial scale climatic oscillations in the central adriatic during the lateglacial: Palaeoceanographic implications. Quat. Sci. Rev. 20, 1201–1221. https://doi.org/10.1016/S0277-3791(00)00147-5

Bé, A.W.H., 1960. Ecology of recent planktonic foraminifera: Part 2: Bathymetric and seasonal distributions in the Sargasso Sea off Bermuda. Micropaleontology 6, 373–392.

Bé, A.W.H, 1977. An ecological, zoogeographic and taxonomic review of recent planktonic foraminifera. In: Ramsay, A.T.S. (Ed.), Oceanic Micropaleontology. Academic Press, London, pp. 1–100

Blockley, S.P.E., Lane, C.S., Hardiman, M., Rasmussen, S.O., Seierstad, I.K., Steffensen, J.P., Svensson, A., Lotter, A.F., Turney, C.S.M., Bronk Ramsey, C., 2012. Synchronisation of palaeoenvironmental records over the last 60,000 years, and an

extended INTIMATE 1 event stratigraphy to 48,000 b2k. Quat. Sci. Rev. 36, 2–10. https://doi.org/10.1016/j.quascirev.2011.09.017

Boussetta, S., Kallel, N., Bassinot, F., Labeyrie, L., Duplessy, J., Caillon, N., Dewilde, F., 2012. Comptes Rendus Geoscience Mg / Ca-paleothermometry in the western Mediterranean Sea on planktonic foraminifer species Globigerina bulloides : Constraints and implications Le pale Globigerina bulloides en Me 344, 267–276. https://doi.org/10.1016/j.crte.2012.02.001

Bout-Roumazeilles, V., Combourieu-Nebout, N., Desprat, S., Siani, G., Turon, J.L., Essallami, L., 2013. Tracking atmospheric and riverine terrigenous supplies variability during the last glacial and the Holocene in central Mediterranean. Clim. Past 9, 1065–1087. https://doi.org/10.5194/cp-9-1065-2013

Bronk-Ramsey, C., 2009. Dealing with Outliers and Offsets in Radiocarbon Dating. Radiocarbon 51, 1023–1045. https://doi.org/10.1017/s0033822200034093

Bronk-Ramsey, C., Lee, S., 2013. Recent and Planned Developments of the Program OxCal. Radiocarbon 55, 720–730. https://doi.org/10.2458/azu_js_rc.55.16215

Buccheri, G., Capretto, G., Di Donato, V., Esposito, P., Ferruzza, G., Pescatore, T., Russo Ermolli, E., Senatore, M.R., Sprovieri, M., Bertoldo, M., Carella, D., Madonia, G., 2002. A high resolution record of the last deglaciation in the southern Tyrrhenian sea: Environmental and climatic evolution. Mar. Geol. 186, 447–470. https://doi.org/10.1016/S0025-3227(02)00270-0

Cacho, I., Grimalt, J.O., Pelejero, C., Canals, M., Sierro, F.J., Flores, J.A., Shackleton, N., 1999. Dansgaard-Oeschger and Heinrich event imprints in Alboran Sea paleotemperatures. Paleoceanography 14, 698–705. https://doi.org/10.1029/1999PA900044

Cacho, I., Grimalt, J.O., Sierro, F.J., Shackleton, N., Canals, M., 2000. Evidence for enhanced Mediterranean thermohaline circulation during rapid climatic coolings. Earth Planet. Sci. Lett. 183, 417–429. https://doi.org/10.1016/S0012-821X(00)00296-X

Calvert, S.E., Nielson, B., Fontugne, M.R., 1992. Evidence from nitrogen isotope ratios for enhanced productivity during formation of eastern Mediterranean sapropels. Nature 359, 223–225. https://doi.org/10.1038/359223a0

Capotondi, L., Morigi, C., 1996. The last deglaciation in the South Adriatic Sea:

Biostratigraphy and paleoceanography. Quat. 9, 679–686.

Capotondi, L., Maria Borsetti, A., Morigi, C., 1999. Foraminiferal ecozones, a high resolution proxy for the late Quaternary biochronology in the central Mediterranean Sea. Mar. Geol. 153, 253–274. https://doi.org/10.1016/S0025-3227(98)00079-6

Carboni, M.G., Bergamin, L., Di Bella, L., Landini, B., Manfra, L., Vesica, P., 2005. Late Quaternary paleoclimatic and paleoenviromental changes in the Tyrrhenian Sea. Quat. Sci. Rev. 24, 2069–2082. https://doi.org/10.1016/j.quascirev.2004.09.009

De Lange, G.J., Thomson, J., Reitz, A., Slomp, C.P., Speranza Principato, M., Erba, E., Corselli, C., 2008. Synchronous basin-wide formation and redox-controlled preservation of a Mediterranean sapropel. Nat. Geosci. 1, 606–610. https://doi.org/10.1038/ngeo283

Di Donato, V., Esposito, P., Russo-Ermolli, E., Scarano, A., Cheddadi, R., 2008. Coupled atmospheric and marine palaeoclimatic reconstructions for the last 35 ka in the Sele Plain-Gulf of Salerno area (southern Italy). Quat. Int. 190, 146–157. https://doi.org/10.1016/j.quaint.2008.05.006

Di Donato, V., Insinga, D.D., Iorio, M., Molisso, F., Rumolo, P., Cardines, C., Passaro, S., 2019. The palaeoclimatic and palaeoceanographic history of the Gulf of Taranto (Mediterranean Sea) in the last 15 ky. Glob. Planet. Change 172, 278–297. https://doi.org/10.1016/j.gloplacha.2018.10.014

Dormoy, I., Peyron, O., Nebout, N.C., Goring, S., Kotthoff, U., Magny, M., Pross, J., 2009. Terrestrial climate variability and seasonality changes in the Mediterranean region between 15000 and 4000 years BP deduced from marine pollen records. Clim. Past 5, 615–632. https://doi.org/10.5194/cp-5-615-2009

Essallami, L., Sicre, M.A., Kallel, N., Labeyrie, L., Siani, G., 2007. Hydrological changes in the Mediterranean Sea over the last 30,000 years. Geochemistry, Geophys. Geosystems 8. https://doi.org/10.1029/2007GC001587

Fairbanks, R.G., Wiebe, P.H., 1980. Foraminifera and chlorophyll maximum: Vertical distribution, seasonal succession, and paleoceanographic significance. Science 209, 1524–1526.

Ferraro, S., Sulli, A., Stefano, E. Di, Giaramita, L., Incarbona, A., Mortyn, P.G., Sprovieri, M., Sprovieri, R., Tonielli, R., Vallefuoco, M., Zizzo, E., Tranchida, G., 2018. Late Quaternary palaeoenvironmental reconstruction of sediment drift accumulation in the

Malta Graben (central Mediterranean Sea). Geo-Marine Lett. 38, 241–258. https://doi.org/https://doi.org/10.1007/s00367-018-0534-x

Fontugne, M.R., Paterne, M., Calvert, S.E., Murat, A., Guichard, F., Arnold, M., 1989. Adriatic deep water formation during the Holocene: implication for the reoxygenation of the deep eastern Mediterranean Sea. Paleoceanography 4, 199–206.

Fontugne, M.R and Calvert, S., 1992. Late Pleistocene variability of the carbon isotopic composition of organic matter in the eastern Mediterranean: Monitor of changes in carbon sources and atmospheric CO2 concentrations. Paleoceanography 7, 1–20. https://doi.org/https://doi.org/10.1029/91PA02674

Fontugne, M., Arnold, M., Labeyrie, L., Paterne, M., Calvert, S.E., Duplessy, J.C., 1994. Paleoenvironment, sapropel chronology and Nile river discharge during the last 20,000 years as indicated by deep-sea sediment records in the eastern Mediterranean. Radiocarbon 34, 75–88.

Gàmiz, M.., Ruiz, F.M., Rampen, S.W., Schouten, S., Damsté, J.S.S., 2014. Sea surface temperature variations in the western Mediterranean Sea over the last 20 kyr: A dual-organic proxy (UK′ 37 and LDI) approach. Paleoceanography 29, 87–98. https://doi.org/10.1002/2013PA002466.Received

Geraga, M., Tsaila-Monopolis, S., Ioakim, C., Papatheodorou, G., Ferentinos, G., 2005. Short-term climate changes in the southern Aegean Sea over the last 48,000 years. Palaeogeogr. Palaeoclimatol. Palaeoecol. 220, 311–332. https://doi.org/10.1016/j.palaeo.2005.01.010

Geraga, M., Mylona, G., Tsaila-Monopoli, S., Papatheodorou, G., Ferentinos, G., 2008. Northeastern Ionian Sea: Palaeoceanographic variability over the last 22 ka. J. Mar. Syst. 74, 623–638. https://doi.org/10.1016/j.jmarsys.2008.05.019

Hayes, A., Kucera, M., Kallel, N., Sbaffi, L., Rohling, E.J., 2005. Glacial Mediterranean sea surface temperatures based on planktonic foraminiferal assemblages. Quat. Sci. Rev. 24, 999–1016. https://doi.org/10.1016/j.quascirev.2004.02.018

Hemleben, C., Spindler, M., Anderson, O.R., 1989. Modern planktonic foraminifera. Springer Science & Business Media. https://doi.org/10.1007/978-1-4612-3544-6

Hernández-almeida, I., Bárcena, M.A., Flores, J.A., Sierro, F.J., Sanchez-vidal, A., Calafat, A., 2011. Marine Micropaleontology Microplankton response to environmental

conditions in the Alboran Sea (Western Mediterranean): One year sediment trap record. Mar. Micropaleontol. 78, 14–24. https://doi.org/10.1016/j.marmicro.2010.09.005

Hodell, D.A., Nicholl, J.A., Bontognali, T.R.R., Danino, S., Dorador, J., Dowdeswell, J.A., Einsle, J., Kuhlmann, H., Martrat, B., Mleneck-Vautravers, M.J., Rodríguez-Tovar, F.J., Röhl, U., 2017. Anatomy of Heinrich Layer 1 and its role in the last deglaciation. Paleoceanography 32, 284–303. https://doi.org/10.1002/2016PA003028

Hutson, W.H., 1980. The Agulhas current during the Late Pleistocene: Analysis of modern faunal analogs. Science (80-.). 207, 64–66. https://doi.org/10.1126/science.207.4426.64

Incarbona, A., Di Stefano, E., Sprovieri, R., Bonomo, S., Censi, P., Dinarès-Turell, J., Spoto, S., 2008. Variability in the vertical structure of the water column and paleoproductivity reconstruction in the central-western Mediterranean during the Late Pleistocene. Mar. Micropaleontol. 69, 26–41. https://doi.org/10.1016/j.marmicro.2007.11.007

Jorissen, F.J., Asioli, A., Borsetti, A.M., Capotondi, L., Visse, J.P. De, Hilgen, F.J., Rohling, E.J., 1993. Late Quaternary central Mediterranean biochronology. MarineMicropaleontology 21, 169–189.

Kallel, N., Paterne, M., Duplessy, J.C., Vergnaud-Grazzini, C., Pujol, C., Labeyrie, L., Arnold, M., Fontugne, M., Pierre, C., 1997a. Enhanced rainfall in the Mediterranean region during the last Sapropel Event. Oceanol. Acta 20, 697–712. https://doi.org/https://archimer.ifremer.fr/doc/00093/20427/

Kallel, N., Paterne, M., Labeyrie, L., Duplessy, J.C., Arnold, M., 1997b. Temperature and salinity records of the Tyrrhenian Sea during the last 18,000 years. Palaeogeogr. Palaeoclimatol. Palaeoecol. 135, 97–108. https://doi.org/10.1016/S0031-0182(97)00021-7

Kallel, N., Duplessy, J.C., Labeyrie, L., Fontugne, M., Paterne, M., 2004. Mediterranean Sea palaeohydrology and pluvial periods during the Late Quaternary. Past Clim. Var. through Eur. Africa 6, 307–324. https://doi.org/https://doi.org/10.1007/978-1-4020-2121-3_15

Kobashi, T., Menviel, L., Jeltsch-thömmes, A., Vinther, B.M., Box, J.E., Muscheler, R., Nakaegawa, T., Pfister, P.L., Döring, M., Leuenberger, M., Wanner, H., Ohmura, A., 2017. Volcanic influence on centennial to millennial Holocene Greenland temperature change. Sci. Rep. 7, 1–10. https://doi.org/10.1038/s41598-017-01451-7

Kotthoff, U., Pross, J., Müller, U.C., Peyron, O., Schmiedl, G., Schulz, H., Bordon, A., 2008.

Climate dynamics in the borderlands of the Aegean Sea during formation of sapropel S1 deduced from a marine pollen record. Quat. Sci. Rev. 27, 832–845. https://doi.org/10.1016/j.quascirev.2007.12.001

Kucera, M., 2007. Planktonic Foraminifera as Tracers of Past Oceanic Environments. Dev. Mar. Geol. 1, 213–262. https://doi.org/10.1016/S1572-5480(07)01011-1

Lionello, P., Malanotte-rizzoli, P., Boscolo, R., Alpert, P., Artale, V., Li, L., Luterbacher, J., May, W., Trigo, R., Tsimplis, M., Ulbrich, U., Xoplaki, E., 2006. The Mediterranean Climate: An overview of the main characteristics and issues. Dev. Earth Environ. Sci. 4, 1–26. https://doi.org/10.1016/S1571-9197(06)80003-0

Lirer, F., Sprovieri, M., Ferraro, L., Vallefuoco, M., Capotondi, L., Cascella, A., Petrosino, P., Insinga, D.D., Pelosi, N., Tamburrino, S., Lubritto, C., 2013. Integrated stratigraphy for the Late Quaternary in the eastern Tyrrhenian Sea. Quat. Int. 292, 71–85. https://doi.org/10.1016/j.quaint.2012.08.2055

Locarnini, R.A., Mishonov, A.V., Baranova, O.K., Boyer, T.P., Zweng, M.M., Garcia, H.E., Reagan, J.R., Seidov, D., Weathers, K.W., Paver, C.R. and Smolyar. I.V., 2019. World Ocean Atlas 2018, Volume 1: Temperature. Mishonov, A., Tech. Ed. NOAA Atlas NESDIS 81, 52pp. https://doi.org/http://www.nodc.noaa.gov/OC5/indprod.html.

Lowe, J.J., Rasmussen, S.O., Björck, S., Hoek, W.Z., Steffensen, J.P., Walker, M.J.C., Yu, Z.C., 2008. Synchronisation of palaeoenvironmental events in the North Atlantic region during the Last Termination: a revised protocol recommended by the INTIMATE group. Quat. Sci. Rev. 27, 6–17. https://doi.org/10.1016/j.quascirev.2007.09.016

Mallo, M., Ziveri, P., Mortyn, P.G., Schiebel, R., Grelaud, M., 2017. Low planktic foraminiferal diversity and abundance observed in a spring 2013 west – east Mediterranean Sea plankton tow transect. Biogeosciences 14, 2245–2266. https://doi.org/10.5194/bg-14-2245-2017

Martrat, B., Jimenez-amat, P., Zahn, R., Grimalt, J.O., 2014. Similarities and dissimilarities between the last two deglaciations and interglaciations in the North Atlantic region. Quat. Sci. Rev. J. 99, 122–134. https://doi.org/https://doi.org/10.1016/j.quascirev.2014.06.016

Melki, T., Kallel, N., Jorissen, F.J., Guichard, F., Dennielou, B., Berné, S., Labeyrie, L., Fontugne, M., 2009. Abrupt climate change, sea surface salinity and paleoproductivity in the western Mediterranean Sea (Gulf of Lion) during the last 28 kyr. Palaeogeogr.

Palaeoclimatol. Palaeoecol. 279, 96–113. https://doi.org/10.1016/j.palaeo.2009.05.005

Melki, T., Kallel, N., Fontugne, M., 2010. The nature of transitions from dry to wet condition during sapropel events in the Eastern Mediterranean Sea Palaeogeogr. Palaeoclimatol. Palaeoecol. 291, 267-285. https://doi.org/10.1016/j.palaeo.2010.02.039

Mercone, D., Thomson, J., Croudace, I.W., Siani, G., Paterne, M., Troelstra, S., 2000. Duration of S1, the most recent sapropel in the eastern Mediterranean Sea, as indicated by accelerator mass spectrometry radiocarbon and geochemical evidence. Paleoceanography 15, 336–347. https://doi.org/10.1029/1999PA000397

Minisini, D., Trincardi, F., Asioli, A., Foglini, F., 2007. Morphologic variability of exposed mass-transport deposits on the eastern slope of Gela Basin (Sicily channel) LT. Basin Res. 19, 217–240. https://doi.org/10.1111/j.1365-2117.2007.00324.x

Mojtahid, M., Manceau, R., Schiebel, R., Hennekam, R., De Lange, G.J., 2015. Thirteen thousand years of southeastern Mediterranean climate variability inferred from an integrative planktic foraminiferal-based approach. Paleoceanography 30, 402–422. https://doi.org/10.1002/2014PA002705

Prell, W.L., 1985. Stability of low-latitude sea-surface temperatures: an evaluation of the CLIMAP reconstruction with emphasis on the positive SST anomalies. Final report.

Principato, M.S., Giunta, S., Corselli, C., Negri, A., 2003. Late Pleistocene-Holocene planktonic assemblages in three box-cores from the Mediterranean Ridge area (west-southwest of Crete): Palaeoecological and palaeoceanographic reconstruction of sapropel S1 interval. Palaeogeogr. Palaeoclimatol. Palaeoecol. 190, 61–77. https://doi.org/10.1016/S0031-0182(02)00599-0

Pujol, C., Vergnaud-Grazzini, C., 1989. Palaeoceanography of the last deglaciation in the Alboran Sea (western Mediterranean). Stable isotopes and planktonic foraminiferal records. Mar. Micropaleontol. 15, 153–179. https://doi.org/10.1016/0377-8398(89)90009-1

Pujol, C., Vergnaud-Grazzini, C., 1995. Distribution patterns of live planktic foraminifers as related to regional hydrography and productive systems of the Mediterranean Sea. Mar. Micropaleontol. 25, 187–217. https://doi.org/10.1016/0377-8398(95)00002-I

Quézel, P., Médail, F., 2003. Ecologie et biogéographie des forêts du bassin méditerranéen. Elsevier-Lavoisier eds, Paris, Fr. 1, 571.

Rasmussen, S.O., Bigler, M., Blockley, S.P., Blunier, T., Buchardt, S.L., Clausen, H.B., Cvijanovic, I., Dahl-Jensen, D., Johnsen, S.J., Fischer, H., Gkinis, V., Guillevic, M., Hoek, W.Z., Lowe, J.J., Pedro, J.B., Popp, T., Seierstad, I.K., Steffensen, J.P., Svensson, A.M., Vallelonga, P., Vinther, B.M., Walker, M.J.C., Wheatley, J.J., Winstrup, M., 2014. A stratigraphic framework for abrupt climatic changes during the Last Glacial period based on three synchronized Greenland ice-core records: Refining and extending the INTIMATE event stratigraphy. Quat. Sci. Rev. 106, 14–28. https://doi.org/10.1016/j.quascirev.2014.09.007

Reimer, P.J., Austin, W.E.N., Bard, E., Bayliss, A., Blackwell, P.G., Bronk Ramsey, C., Butzin, M., Cheng, H., Edwards, R.L., Friedrich, M., Grootes, P.M., Guilderson, T.P., Hajdas, I., Heaton, T.J., Hogg, A.G., Hughen, K.A., Kromer, B., Manning, S.W., Muscheler, R., Palmer, J.G., Pearson, C., van der Plicht, J., Reimer, R.W., Richards, D.A., Scott, E.M., Southon, J.R., Turney, C.S.M., Wacker, L., Adolphi, F., Büntgen, U., Capano, M., Fahrni, S.M., Fogtmann-Schulz, A., Friedrich, R., Köhler, P., Kudsk, S., Miyake, F., Olsen, J., Reinig, F., Sakamoto, M., Sookdeo, A., Talamo, S., 2020. THE INTCAL20 NORTHERN HEMISPHERE RADIOCARBON AGE CALIBRATION CURVE (0–55 CAL kBP). Radiocarbon 00, 1–33. https://doi.org/10.1017/rdc.2020.41

Revel, M., Ducassou, E., Grousset, F.E., Bernasconi, S.M., Migeon, S., Revillon, S., Mascle, J., Murat, A., Zaragosi, S., Bosch, D., 2010. 100 , 000 Years of African monsoon variability recorded in sediments of the Nile margin. Quat. Sci. Rev. J. 29, 1342–1362. https://doi.org/10.1016/j.quascirev.2010.02.006

Rigual-Hernández, A.S., Sierro, F.J., Bárcena, M.A., Flores, J.A., Heussner, S., 2012. Seasonal and interannual changes of planktic foraminiferal fluxes in the Gulf of Lions (NW Mediterranean) and their implications for paleoceanographic studies : Two 12-year sediment trap records. Deep. Res. Part I Oceanogr. Res. Pap. 66, 26–40. https://doi.org/10.1016/j.dsr.2012.03.011

Rogerson, M., Rohling, E.J., Weaver, P.P.E., Murray, J.W., 2004. The Azores Front since the Last Glacial Maximum. Earth Planet. Sci. Lett. 222, 779–789. https://doi.org/10.1016/j.epsl.2004.03.039

Rohling, E.J., Gieskes, W.W.C., 1989. Late Quaternary changes in Mediterranean intermediate water density and formation rate. Paleoceanography 4, 531–545. https://doi.org/10.1029/PA004i005p00531

Rohling, E.J., Jorissen, F.J., Grazzini, C.V., Zachariasse, W.J., 1993. Northern Levantine and Adriatic Quaternary planktic foraminifera; Reconstruction of paleoenvironmental gradients. Mar. Micropaleontol. 21, 191–218. https://doi.org/10.1016/0377-8398(93)90015-P

Rohling, E.J., 1994. Review and new aspects concerning the formation of eastern Mediterranean sapropels. Mar. Geol. 122, 1–28. https://doi.org/10.1016/0025-3227(94)90202-X

Rohling, E.J., Jorissen, F.J., De Stigter, H.C., 1997. 200 Year interruption of Holocene sapropel formation in the Adriatic Sea. J. Micropalaeontology 16, 97–108. https://doi.org/10.1144/jm.16.2.97

Rohling, E., Mayewski, P., Abu-Zied, R., Casford, J., Hayes, A., 2002. Holocene atmosphere-ocean interactions: Records from Greenland and the Aegean sea. Clim. Dyn. 18, 587–594. https://doi.org/10.1007/s00382-001-0194-8

Rossignol-Strick, M., Nesteroff, W., Olive, P., Vergnaud-Grazzini, C., 1982. After the deluge: Mediterranean stagnation and sapropel formation. Nature 295, 105–110. https://doi.org/10.1038/295105a0

Rouis-Zargouni, I., Turon, J.L., Londeix, L., Essallami, L., Kallel, N., Sicre, M.A., 2010. Environmental and climatic changes in the central Mediterranean Sea (Siculo-Tunisian Strait) during the last 30 ka based on dinoflagellate cyst and planktonic foraminifera assemblages. Palaeogeogr. Palaeoclimatol. Palaeoecol. 285, 17–29. https://doi.org/10.1016/j.palaeo.2009.10.015

Sbaffi, L., Wezel, F.C., Kallel, N., Paterne, M., Cacho, I., Ziveri, P., Shackleton, N., 2001. Response of the pelagic environment to palaeoclimatic changes in the central Mediterranean Sea during the Late Quaternary. Mar. Geol. 178, 39–62. https://doi.org/10.1016/S0025-3227(01)00185-2

Sbaffi, L., Wezel, F.C., Curzi, G., Zoppi, U., 2004. Millennial- to centennial-scale palaeoclimatic variations during Termination I and the Holocene in the central Mediterranean Sea. Glob. Planet. Change 40, 201–217. https://doi.org/10.1016/S0921-8181(03)00111-5

Schiebel, R., Hemleben, C., 2005. Modern planktic foraminifera. Paläontologische Zeitschrift 79, 135–148. https://doi.org/10.1007/bf03021758

Schiebel, R., Hemleben, C., 2017. Planktic Foraminifers in the Modern Ocean, Springer. https://doi.org/10.1007/978-3-662-50297-6

Siani, G., Paterne, M., Arnold, M., Bard, E., Métivier, B., Tisnerat, N., Bassinot, F., 2000. Radiocarbon reservoir ages in the Mediterranean Sea and Black Sea. Radiocarbon 42, 271–280. https://doi.org/10.1017/S0033822200059075

Siani, G., Paterne, M., Michel, E., Sulpizio, R., Sbrana, A., Arnold, M., Haddad, G., 2001. Mediterranean sea surface radiocarbon reservoir age changes since the last glacial maximum. Science (80). 294, 1917–1920. https://doi.org/10.1126/science.1063649

Siani, G., Paterne, M., Colin, C., 2010. Late glacial to Holocene planktic foraminifera bioevents and climatic record in the South Adriatic Sea. J. Quat. Sci. 25, 808–821. https://doi.org/10.1002/jqs.1360

Siani, G., Magny, M., Paterne, M., Debret, M., Fontugne, M., 2013. Paleohydrology reconstruction and Holocene climate variability in the South Adriatic Sea. Clim. Past 9, 499–515. https://doi.org/10.5194/cp-9-499-2013

Siccha, M., Kucera, M., 2017. Data Descriptor : ForCenS , a curated database of planktonic foraminifera census counts in marine surface sediment samples. Nature 1–12.

Sierro, F.J., Hodell, D.A., Curtis, J.H., Flores, J.A., Reguera, I., Colmenero-Hidalgo, E., Bárcena, M.A., Grimalt, J.O., Cacho, I., Frigola, J., Canals, M., 2005. Impact of iceberg melting on Mediterranean thermohaline circulation during Heinrich events. Paleoceanography 20, 1–13. https://doi.org/10.1029/2004PA001051

Sprovieri, R., Di Stefano, E., Incarbona, A., Gargano, M.E., 2003. A high-resolution record of the last deglaciation in the Sicily Channel based on foraminifera and calcareous nannofossil quantitative distribution. Palaeogeogr. Palaeoclimatol. Palaeoecol. 202, 119–142. https://doi.org/10.1016/S0031-0182(03)00632-1

Sprovieri, M., Di Stefano, E., Incarbona, A., Salvagio Manta, D., Pelosi, N., Ribera d'Alcalà, M., Sprovieri, R., 2012. Centennial- to millennial-scale climate oscillations in the Central-Eastern Mediterranean Sea between 20,000 and 70,000 years ago: Evidence from a high-resolution geochemical and micropaleontological record. Quat. Sci. Rev. 46, 126–135. https://doi.org/10.1016/j.quascirev.2012.05.005

Stuiver, M., Polach, H.A., 1977. Discussion Reporting of 14C Data. Radiocarbon 19, 355–363. https://doi.org/10.1017/S0033822200003672

Therón, R., Paillard, D., Cortijo, E., Flores, J., Sierro, F.J., Waelbroeck, C., Thern, R., Paillard, D., Cortijo, E., Vaquero, M., Sierro, F.J., Waelbroeck, C., 2004. Rapid Reconstruction of Paleoenvironmental Features Using a New Multiplatform Program Short Note Rapid reconstruction of paleoenvironmental features using a new multiplatform program. Micropaleontology 50, 391–395. https://doi.org/https://doi.org/10.2113/50.4.391

Tisnérat-Laborde, N., Poupeau, J.J., Tannau, J.F., Paterne, M., 2001. Development of a Semi-Automated System for Routine Preparation of Carbonate Samples. Radiocarbon 43, 299–304. https://doi.org/10.1017/s0033822200038145

Tisnérat-Laborde, N., Thil, F., Synal, H.A., Cersoy, S., Hatté, C., Gauthier, C., Massault, M., Michelot, J.L., Noret, A., Siani, G., others, 2015. ECHoMICADAS: A new compact AMS system to measuring 14C for environment, climate and human sciences, in: 22nd International Radiocarbon Conference. Dakar, Senegal. pp. 16–20.

Tolderlund, D.S., Bé, A.W.H., 1971. Seasonal distribution of planktonic foraminifera in the western North Atlantic. Micropaleontology 17, 297–329. https://doi.org/https://doi.org/10.2307/1485143

Triantaphyllou, M. V., Antonarakou, A., Kouli, K., Dimiza, M., Kontakiotis, G., Papanikolaou, M.D., Ziveri, P., Mortyn, P.G., Lianou, V., Lykousis, V., Dermitzakis, M.D., 2009. Late Glacial-Holocene ecostratigraphy of the south-eastern Aegean Sea, based on plankton and pollen assemblages. Geo-Marine Lett. 29, 249–267. https://doi.org/10.1007/s00367-009-0139-5

Vergnaud-Grazzini, C., Borsetti, A.M., Cati, F., Colantoni, P., D'Onofrio, S., Saliège, J.F., Sartori, R., Tampieri, R., 1988. Palaeoceanographic record of the Last deglaciation in the Strait of Sicily. Mar. Micropaleontol. 13, 1–21. https://doi.org/https://doi.org/10.1016/0377-8398(88)90010-2

Wacker, L., Fahrni, S.M., Hajdas, I., Molnar, M., Synal, H.A., Szidat, S., Zhang, Y.L., 2013. A versatile gas interface for routine radiocarbon analysis with a gas ion source. Nucl. Instruments Methods Phys. Res. Sect. B Beam Interact. with Mater. Atoms 294, 315–319. https://doi.org/10.1016/j.nimb.2012.02.009

Walker, M., Head, M.J., Berkelhammer, M., Björck, S., Cheng, H., Cwynar, L., Fisher, D., Gkinis, V., Long, A., Lowe, J., Newnham, R., Rasmussen, S.L., Weiss, H., 2018. Formal ratification of the subdivision of the Holocene Series/ Epoch (Quaternary

System/Period): two new Global Boundary Stratotype Sections and Points (GSSPs) and three new stages/ subseries. Episodes, 41, 213-223

WOA, 1998. World ocean atlas 1998, version 2, http://www.nodc. noaa.gov/oc5/woa98.html. Technical Report, National Oceanographic Data Center, Silver Spring, Maryland

Young, N.E., Briner, J.P., Miller, G.H., Lesnek, A.J., Crump, S.E., Thomas, E.K., Pendleton, S.L., Cuzzone, J., Lamp, J., Zimmerman, S., Caffee, M., Schaefer, J.M., 2020. Deglaciation of the Greenland and Laurentide ice sheets interrupted by glacier advance during abrupt coolings. Quat. Sci. Rev. 229. https://doi.org/10.1016/j.quascirev.2019.106091

Data Citations

CLIMAP Project Members. PANGAEA https://doi.org/10.1594/PANGAEA.51927 (2009).

Prell, W., Martin, A., Cullen, J. & Trend, M. NOAA https://www.ncdc.noaa.gov/paleo-search/study/5908 (1999).

Pflaumann, U. et al. PANGAEA https://doi.org/10.1594/PANGAEA.77352 (2003).

Kucera, M. et al. PANGAEA https://doi.org/10.1594/PANGAEA.227322 (2005).

Hayes, A., Kucera, M., Kallel, N., Sbaffi, L. & Rohling, E. PANGAEA https://doi.org/10.1594/PANGAEA.738564 (2005)

Hüls, M. PANGAEA https://doi.org/10.1594/PANGAEA.55758 (1999).

Mohtadi, M., Hebbeln, D. & Marchant, M. PANGAEA https://doi.org/10.1594/PANGAEA.351143 (2005).

Mohtadi, M. PANGAEA https://doi.org/10.1594/PANGAEA.733339 (2010)

Salgueiro, E. et al. PANGAEA https://doi.org/10.1594/PANGAEA.743252 (2008)

Siccha, M., Trommer, G., Schulz, H., Hemleben, C. & Kucera, M. PANGAEA https://doi.org/10.1594/PANGAEA.877924 (2017).

Munz, P. et al. PANGAEA https://doi.org/10.1594/PANGAEA.853966 (2015).

Figure 1: Map of the Mediterranean annual mean SSTs (°C, 1955-2012) from Word Ocean Atlas 2013 (http://odv.awi.de/de/data/ocean/world ocean atlas 2013 /) showing the locations of studiedcores: REC13-53, KET80-19, MD84-641 (Red diamonds) and the others

Mediterranean records mentioned in the text: Hole 963D (Sprovieri et al., 2003); BS79-22 (Sbaffi et al., 2001); BS79-38 (Sbaffi et al., 2004); C69 (Geraga et al., 2005); GNS84-C106 (Di Donato et al., 2008); NS-14 (Triantaphyllou et al., 2009) (Purple diamonds).

Figure 2: a) Variations in oxygen isotope ($\delta^{18}O$) of the planktonic foraminifera *Globigerina bulloides* vs. depth. b) Age-depth relation for REC13-53 core based on 13 AMS^{14}C dates.

Figure 3: Comparison of palaeoclimatic record from REC13-53 core and Greenland ice-core over the last 24 kyr BP. (a) Oxygen isotope record from NGRIP ice core and event stratigraphy protocol recommended by the INTIMATE group (GS-2, Greenland stadial 2 (GS-2a–c are sub-stadials); GI-1,Greenland Interstadial 1 (GI-1a–e are sub-interstadials); GS-1, Greenland Stadial 1; Lowe et al., 2008) and the corresponding main climatic transitions (sensu Mangerud et al., 1974). (b) SST fluctuations generated by modern analogue technique. (c) Dissimilarity coefficient record. (d) Variations in oxygen isotope ($\delta^{18}O$) of the planktonic foraminifera *Globigerina bulloides*.

Figure 4: a) Relative abundances of planktic foraminiferal assemblages in REC13-53 core vs. age (cal. Kyr BP), b) Relative abundances of planktic foraminiferal assemblages in KET80-19 core, c) Relative abundances of planktic foraminiferal assemblages in MD84-641 core.

Figure 5: a) Annual SST (°C) by MAT in REC13-53 core, b) Dissimilarity coefficient in REC13-53 core, c) Annual SST (°C) by MAT in KET80-19 core, d) Dissimilarity coefficient in KET80-19 core, e) Annual SST (°C) by MAT in MD84-641 core and, f) Dissmilarity coefficient in MD84-641 core. The red star represents the present day temperature at the location of each core.

Figure 6: Comparison between the biochronological schemes developed in this study with previous reconstructions in the adjacent basins (Sprovieri et al., 2003; Sbaffi et al., 2001; Sbaffi et al., 2004; Geraga et al., 2005; Di Donato et al., 2008; Triantaphyllou et al., 2009).

Table 1. Summary of the core details used in this paper

Core name	Location	Long.	Lat.	Water depth (m)
REC13-53	Siculo-Tunisian	12°08'E	36°45'N	1113

	Strait			
KET80-19	Tyrrhenian Sea	13°21'E	40°33'N	1920
MD84-641	Levantine Basin	32°38'E	33°02'N	1375

*****Long.: Longitude *Lat.: Latitude *m: meter

Table 2. AMS radiocarbon dating obtained for REC13-53, KET80-19 and MD84-641 cores.

code	Core	Depth (cm)	Conventional Radiocarbon Age	Standard deviation (±1σ)	Corrected 14C Age	Median Cal Age (yr BP)	Error median Age (2σ)	Material
ECHo2533	REC	9-10	1260	40	860	771	907-691	*G. bulloides*
ECHo2535	13-53	117-	5660	45	5260	6032	6180-5925	*G. ruber alba*
ECHo2537		118	6925	45	6525	7451	7562-7332	*G. ruber alba*
ECHo2199		149-	8190	60	7790	8557	8697-8421	*G. ruber alba*
ECHo2539		150	8845	50	8445	9435	9525-9296	*G. ruber alba*
ECHo3276		165-	8870	80	8470	9577	9762-9446	*G. ruber alba*
ECHo2197		166	9820	70	9420	10653	11000-10438	*G. bulloides*
ECHo2195		181-	10680	70	10280	11917	12152-11716	*G. bulloides*
ECHo3278		182	10740	70	10370	12411	12614-12166	*N. incompta*
ECHo3282		189-	12470	80	12070	13995	14278-13745	*G. ruber alba*
ECHo3284		190	13095	125	12495	14583	15016-14215	*G. ruber alba*
ECHo3288		213-	17090	120	16690	20286	20708-19858	*G. bulloides*
SacA17148		214	19510	190	19110	23027	23485-22574	*G. bulloides*
		241-						
		242						
		257-						
		258						
		289-						
		290						
		301-						
		302						
		425-						
		470						
		485-						
		486						
	KET	45	4320	60	3920	4351	4506-4235	Tephra/KET80-
	80-19	55	5270	70	4870	5608	5748-5333	19
		68	6030	70	5630	6421	6615-6293	*G. bulloides*
		78	7220	80	6820	7697	7845-7570	*G. bulloides*
		80	7000	50	7400	7816	7932-7702	*G. bulloides*
		88	8350	80	7950	8794	9003-8597	Tephra
		103	9550	90	9150	10286	10517-9932	*G. bulloides*
		140	9800	50	10200	11224	11318-11163	*G. bulloides*
		148	10700	160	10300	11944	12516-11358	Tephra
		180	12300	50	12700	14239	14601-14054	correlation with KET80-03 $\delta^{18}O$
		220	14400	100	14800	17500	17789-17176	Tephra
		261	16000	160	15600	18935	19361-18607	Tephra
		301	18740	200	18340	22154	22572-21689	correlation with KET80-03 $\delta^{18}O$ correlation with KET80-03 $\delta^{18}O$

	MD 84-641	1	4220	110	3820	4124	4415-3868	*G. ruber*
		13	4390	120	3990	4640	4851-4315	*G. ruber*
		22	6710	100	6310	7261	7435-7001	*G. ruber*
		24	7070	100	6670	7530	7691-7332	*G. ruber*
		28	7490	100	7090	7910	8155-7697	*G. ruber*
		32	8200	130	7800	8585	8957-8375	*G. ruber*
		37	8450	130	8050	8998	9295-8648	*G. ruber*
		40	8700	110	8300	9296	9493-9032	*G. ruber*
		43	9760	130	9360	10545	11054-10234	*G. ruber*
		48	10120	150	9720	11103	11603-10690	*G. ruber*
		57	11990	200	11590	13310	13671-13001	*G. ruber*
		65	12120	180	11720	13700	14107-13362	*G. ruber*
		75	14800	260	14400	17505	18141-16784	*G. ruber*
		85	17170	270	16770	20195	20811-19567	*G. ruber*
		95	18500	270	18100	21889	22469-21167	*G. ruber*

Highlights

- We present a high-resolution biochronological records in the Mediterranean Sea
- Seven biozones are identified basing on the distributional patterns of planktic foraminifera
- Four bio-events were recognized, and they should improve the chronology of Mediterranean cores
- A similarity between the global climate and the Mediterranean hydrology is observed

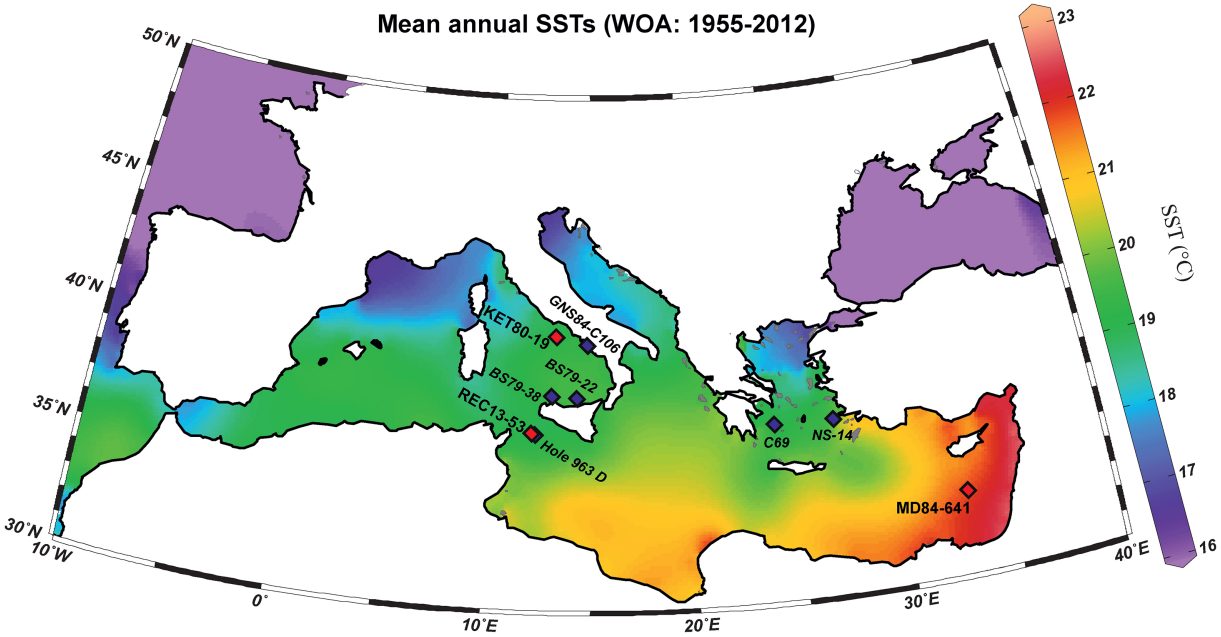
Mean annual SSTs (WOA: 1955-2012)
50°N
45°N
40°N
35°N
30°N
10°W
0°
10°E
20°E
30°E
40°E
KET80-19
GNS84-C106
BS79-22
BS79-38
REC13-53
Hole 963 D
C69
NS-14
MD84-641
SST (°C)
23
22
21
20
19
18
17
16

Figure 1

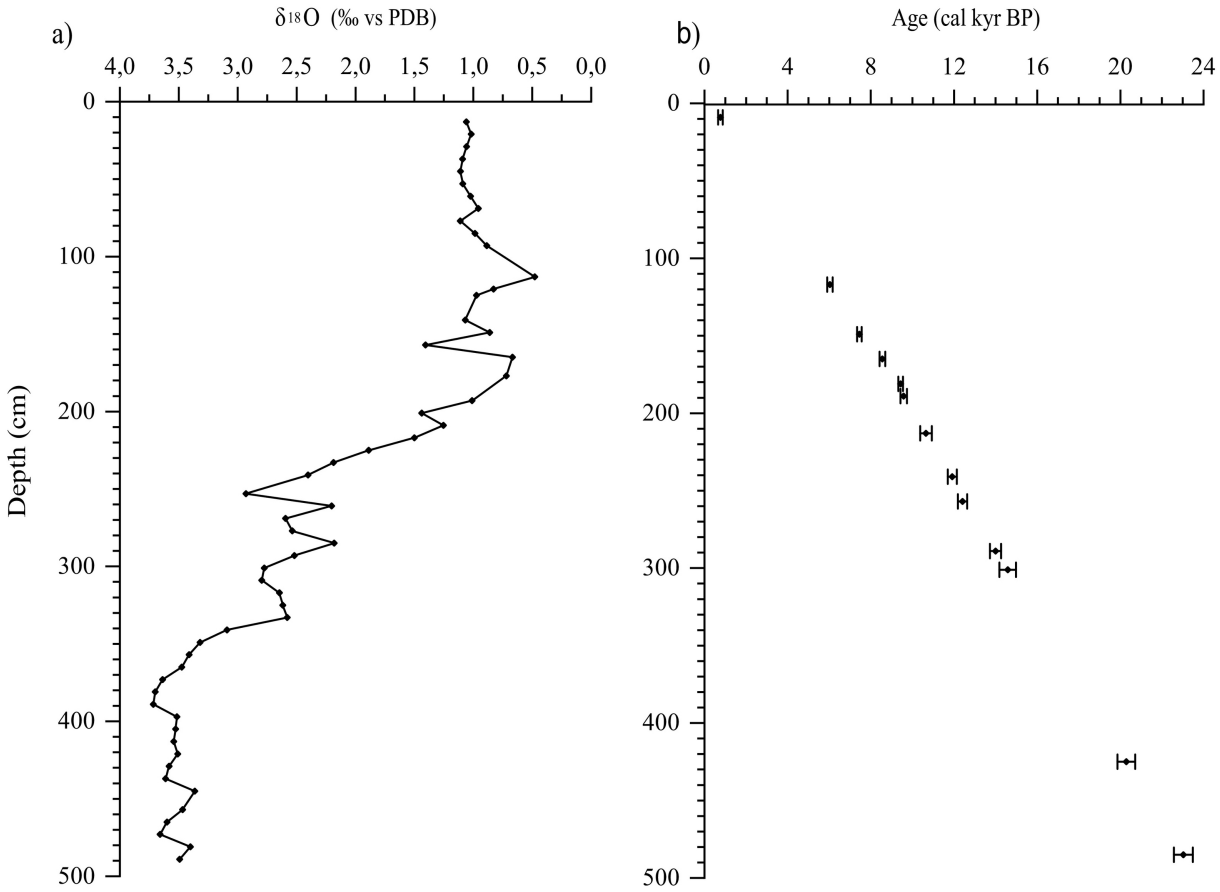
a)
δ18O (‰ vs PDB)
4,0
3,5
3,0
2,5
2,0
1,5
1,0
0,5
0,0
b)
Age (cal kyr BP)
0
4
8
12
16
20
24
Depth (cm)
0
100
200
300
400
500

Figure 2

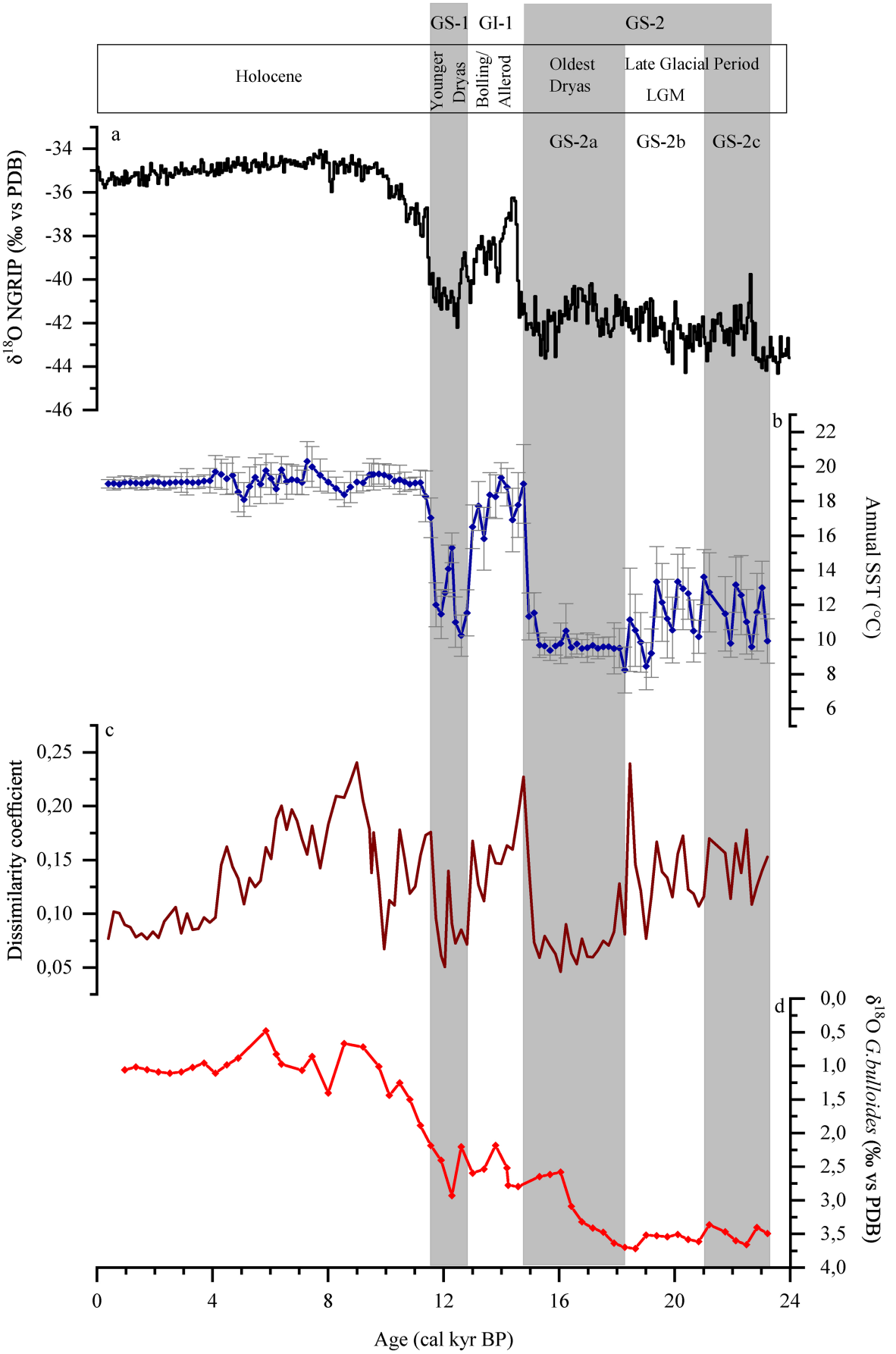
GS-1
GI-1
GS-2
Holocene
Younger Dryas
Bolling/ Allerod
Oldest Dryas
Late Glacial Period
LGM
GS-2a
GS-2b
GS-2c
a
δ18O NGRIP (‰ vs PDB)
-34
-36
-38
-40
-42
-44
-46
b
Annual SST (°C)
22
20
18
16
14
12
10
8
6
c
Dissimilarity coefficient
0,25
0,20
0,15
0,10
0,05
d
δ18O G.bulloides (‰ vs PDB)
0,0
0,5
1,0
1,5
2,0
2,5
3,0
3,5
4,0
0
4
8
12
16
20
24
Age (cal kyr BP)

Figure 3

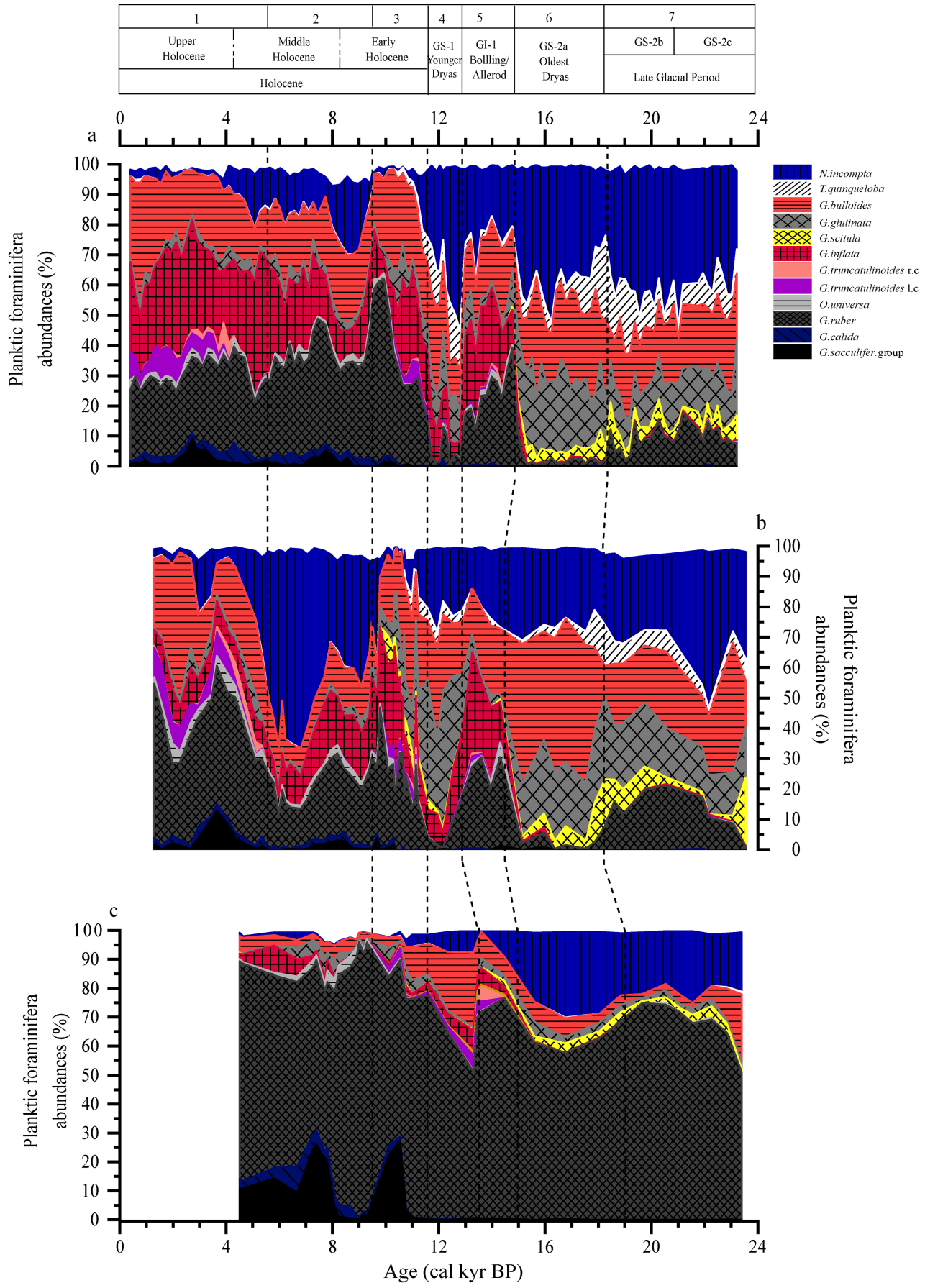
1
2
3
4
5
6
7
Upper Holocene
Middle Holocene
Early Holocene
GS-1 Younger Dryas
GI-1 Bollling/ Allerod
GS-2a Oldest Dryas
GS-2b
GS-2c
Holocene
Late Glacial Period
a
b
c
Planktic foraminifera abundances (%)
N.incompta
T.quinqueloba
G.bulloides
G.glutinata
G.scitula
G.inflata
G.truncatulinoides r.c
G.truncatulinoides l.c
O.universa
G.ruber
G.calida
G.sacculifer. group
Age (cal kyr BP)

Figure 4

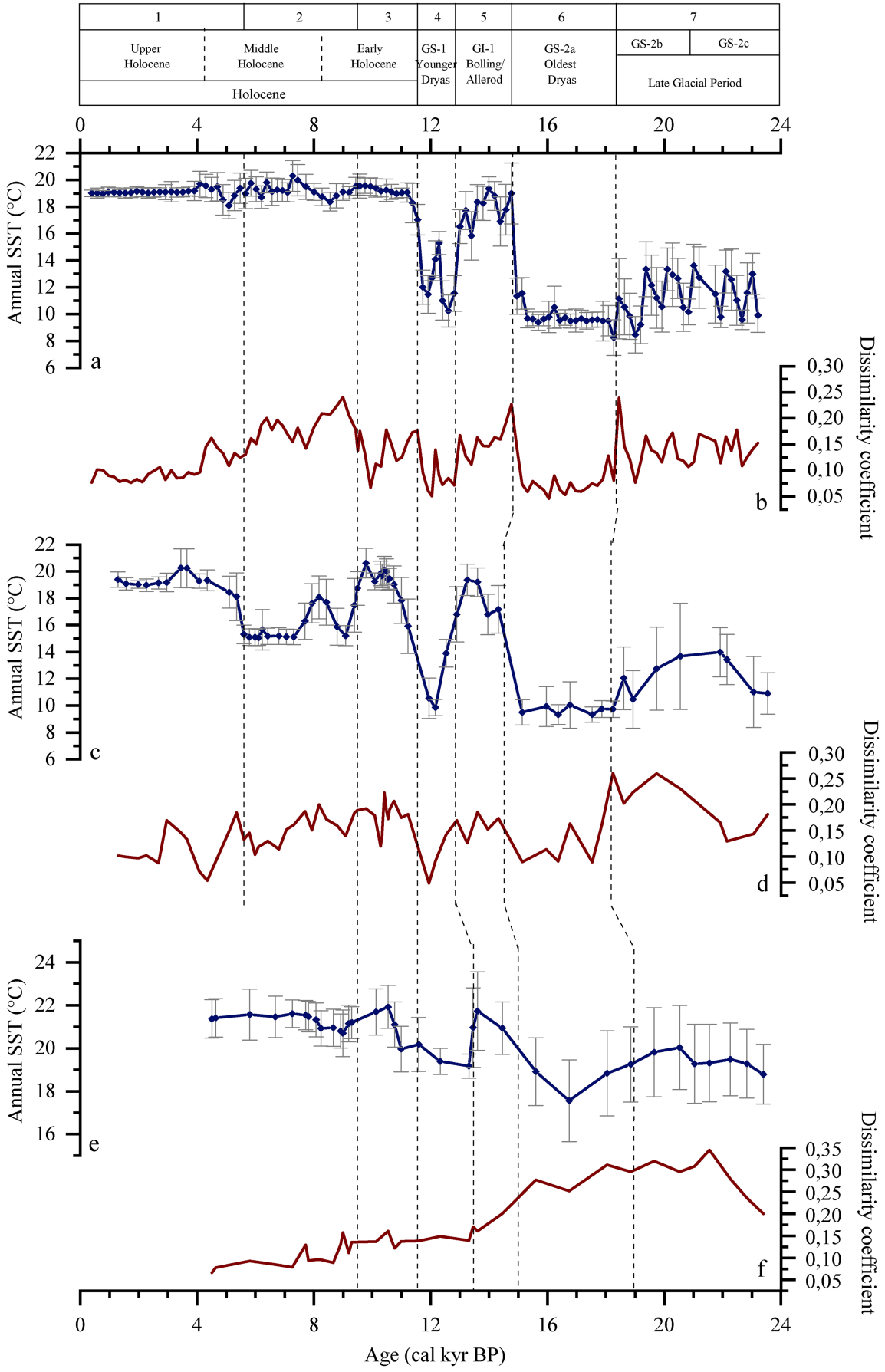
1
2
3
4
5
6
7
Upper Holocene
Middle Holocene
Early Holocene
GS-1 Younger Dryas
GI-1 Bolling/ Allerod
GS-2a Oldest Dryas
GS-2b
GS-2c
Holocene
Late Glacial Period
Annual SST (°C)
Dissimilarity coefficient
a
b
c
d
e
f
Age (cal kyr BP)

Figure 5

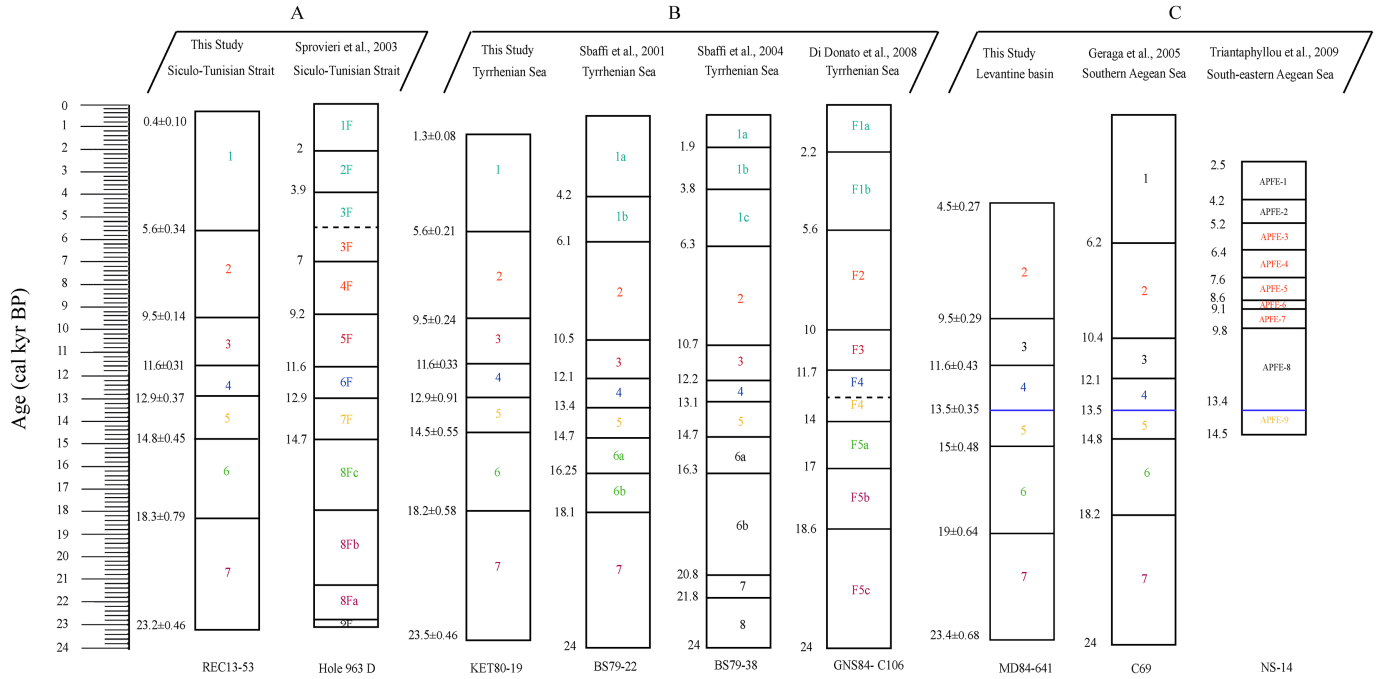
A
B
C
This Study
Siculo-Tunisian Strait
Sprovieri et al., 2003
Siculo-Tunisian Strait
This Study
Tyrrhenian Sea
Sbaffi et al., 2001
Tyrrhenian Sea
Sbaffi et al., 2004
Tyrrhenian Sea
Di Donato et al., 2008
Tyrrhenian Sea
This Study
Levantine basin
Geraga et al., 2005
Southern Aegean Sea
Triantaphyllou et al., 2009
South-eastern Aegean Sea
Age (cal kyr BP)
0
1
2
3
4
5
6
7
8
9
10
11
12
13
14
15
16
17
18
19
20
21
22
23
24
0.4±0.10
5.6±0.34
9.5±0.14
11.6±0.31
12.9±0.37
14.8±0.45
18.3±0.79
23.2±0.46
1
2
3
4
5
6
7
2
3.9
7
9.2
11.6
12.9
14.7
1F
2F
3F
3F
4F
5F
6F
7F
8Fc
8Fb
8Fa
9F
1.3±0.08
5.6±0.21
9.5±0.24
11.6±0.33
12.9±0.91
14.5±0.55
18.2±0.58
23.5±0.46
1
2
3
4
5
6
7
4.2
6.1
10.5
12.1
13.4
14.7
16.25
18.1
24
1a
1b
2
3
4
5
6a
6b
7
1.9
3.8
6.3
10.7
12.2
13.1
14.7
16.3
20.8
21.8
24
1a
1b
1c
2
3
4
5
6a
6b
7
8
2.2
5.6
10
11.7
14
17
18.6
24
F1a
F1b
F2
F3
F4
F4
F5a
F5b
F5c
4.5±0.27
9.5±0.29
11.6±0.43
13.5±0.35
15±0.48
19±0.64
23.4±0.68
2
3
4
5
6
7
6.2
10.4
12.1
13.5
14.8
18.2
24
1
2
3
4
5
6
7
2.5
4.2
5.2
6.4
7.6
8.6
9.1
9.8
13.4
14.5
APFE-1
APFE-2
APFE-3
APFE-4
APFE-5
APFE-6
APFE-7
APFE-8
APFE-9
REC13-53
Hole 963 D
KET80-19
BS79-22
BS79-38
GNS84- C106
MD84-641
C69
NS-14

Figure 6